Communication

Targeted Clinical Nanoparticles for Precision Cancer Therapy based on Disease-specific Molecular Inflection Points

Charalambos Kaittanis, Alexander Bolaender, Barney Yoo, Nilesh Shah, Ouathek Ouerfelli, and Jan Grimm

Nano Lett., **Just Accepted Manuscript** • DOI: 10.1021/acs.nanolett.7b04209 • Publication Date (Web): 16 Oct 2017

Targetable Clinical Nanoparticles for Precision Cancer Therapy based on Disease-specific Molecular Inflection Points

Charalambos Kaittanis[1], Alexander Bolaender[1], Barney Yoo[2**], Nilesh Shah***[2] Ouathek Ouerfelli[2] Jan Grimm[1,3,5]*

[1]Molecular Pharmacology Program, [2]Organic Synthesis Core, Chemical Biology Program,

[3]Department of Radiology, Memorial Sloan Kettering Cancer Center, 1275 York Avenue, New York, NY 10065, USA

[4]Department of Pharmacology and Radiology, Weill Cornell Medical College, New York, NY 10065, USA

*Current address: Gordon Center for Medical Imaging Sciences, Department of Radiology, Massachusetts General Hospital, 55 Fruit Street, Boston, MA 02114.
**Current address: Department of Chemistry, Hunter College, New York, NY 10065
*** Current address: L'Oreal, Bridgewater, New Jersey

ABSTRACT. Novel translational approaches based on clinical modular nanoplatforms are needed, in order to treat solid cancers according to their discrete molecular features. In the present study, we show that the clinical nanopharmaceutical Ferumoxytol, which consists of a glucose-based coat surrounding an iron oxide core, could identify molecular characteristics of prostate cancer, corresponding to unique phases of the disease continuum. By affixing a targeting probe for the prostate-specific membrane antigen on its surface, the nanopharmaceutical was able to assess the functional state of the androgen receptor pathway via MRI, guiding therapy and delivering it with the same clinical nanoparticle. In order to simultaneously inhibit oncogenic signaling from key oncogenic pathways of more advanced forms of prostate cancer, a single-agent therapy for early-stage disease to inhibit DNA replication, as well as combination therapy with two drugs co-retained within the nanopharmaceutical's polymeric coating, were tested, and resulted complete tumor ablation. Recalcitrant and terminal forms of the disease were effectively treated with a nanoparmaceutical delivering a combination that upregulates endoplasmic reticulum stress and inhibits metastasis, thereby showing that this multifunctional nanoplatfom can be used in the clinic for patient stratification, as well as precision treatment based on the individual's unique disease features.

KEYWORDS. molecular imaging, combination therapy, PSMA.

Cancer causes significant mortality throughout the world, mainly as a result of the disease being diagnosed too late, relapsing into an advanced resistant form, or metastasizing to other organs. Therefore, having sensitive diagnostics that can identify early enough cancer hallmarks is critical for treatment, and translates to improved patient survival[1-3]. Similarly, addressing cancer heterogeneity and its complex molecular signaling cascades with carefully selected drug combinations can prevent resistance[4, 5]. However, existing chemotherapeutics are often associated with severe toxicities and off-target effects. For instance, these adverse effects are observed because healthy cells may express a drug's target, cells responsible for important immune functions may uptake the therapeutic, or simply when the drug is retained by excretory

organs, such as the kidneys and liver[6, 7]. Therefore, it is critical to achieve delivery of the drug at the tumor site, ideally using a transport vehicle that has long blood circulation time, can target the pathology, is relatively benign, and consists of clinically approved components. We previously showed that Ferumoxytol (Feraheme), a formulation of iron oxide nanoparticles approved for the treatment of iron deficiency anemia in patients with chronic kidney disease, could serve as a drug delivery vehicle for several chemotherapeutics[8]. Furthermore, we demonstrated that nanophores consisting of dextran but lacking a metal oxide core could similarly retain drugs and radionuclides via weak electrostatic interactions, and deliver their therapeutic cargo to tumors, through the enhanced permeability and retention effect[9].

Since prostate cancer (PC) is typically associated with resistance and recurrence, we used it as a model disease for combination therapy. We also selected PC because of its high prevalence (1 in 7 men will be diagnosed with the disease in their lifetime), and its unique molecular characteristics, including signaling pathway crosstalk[10, 11]. For instance, it was recently demonstrated that inhibition of the androgen receptor upregulates the PI3K pathway[10], as well as the cell surface levels of the prominent cell surface biomarker folate hydrolase 1 (FOLH1, also named PSMA, Gene ID: 2346)[12-14]. PSMA expression is a predictor for PC progression[15] and prognosis[16] of PC, since elevated FOLH1/PSMA levels are seen in aggressive form, such as metastatic and higher-grade PC. Also, tumors with strong *FOLH1* expression have higher risk of biochemical recurrence than cancers with only weak staining intensity[17]. Therefore, we hypothesized that PSMA-targeting multifunctional nanopharmaceuticals are amenable to effective precision therapy, by concomitant diagnosis and treatment based on distinct disease-specific molecular phases that govern the biomarker's expression, achieving tumor regression, averting adverse effects, and preventing resistance and relapse.

Similar to breast and lung cancer, PC evolves and develops resistance, which hinders effective treatment[18, 19]. Specifically, once diagnosed via digital exam or elevated levels of the prostate-specific antigen (PSA), treatment of non-metastatic PC involves surgery to remove the prostate gland, followed by chemo-hormonal therapy that inhibits proliferation signaling, including suppression of the androgen receptor activity (**Figure 1A**). Subsequently, a second

phase usually emerges with time that leads to disease relapse with regrowth that requires treatment with second-generation drugs, such as enzalutamide (Xtandi) and abiraterone acetate (Zytiga), which interfere with AR signaling in order to overcome disease hallmarks, such as amplification of the androgen receptor gene. Although this may lead to transient tumor regression, PC frequently relapses, as a result of acquiring resistance through other metastatic mechanisms, which ultimately cause death. Taking these unique phases in consideration, we sought to develop a nanopharmaceutical that can target PC with therapeutic combinations that target each molecular stage of the disease. Specifically, based on our prior work, we reasoned that Ferumoxytol could be loaded with drugs within its carboxymethyl dextran coating via weak electrostatic interactions, and deliver them with high specificity to PSMA-expressing PC (**Figure 1B**). To achieve this, we conjugated a small cyclical PSMA-targeting peptide to Ferumoxytol, which was previously identified through the panning of a phage display library and binds within the lumen-facing side of PSMA (**SI Figure 1**)[20]. The resulting targeting nanopharmaceutical (TNP) had similar diameter and size distribution to nascent Ferumoxytol (d = 36 nm) that were determined with dynamic light scattering, whereas loading of TNP's with molecular payload, such as the near-infrared fluorophore DiR and doxorubicin, did not affect the nanoparticles' size (**SI Figure 2A**). Conjugation of the peptide to Ferumoxytol (ζ potential = - 40 mV) was reflected in increases in the resulting TNP's surface charge, with the coating-loaded cargo having no effect on this parameter (**SI Figure 2B**). Additional characterization showed that the TNP stably retained their cargo in serum at 37º C for more than a week (**SI Figure 2C**), and could quickly release their payload upon mild acidification of their local surrounding, while withholding it within the coating's amphipathic pockets at neutral pH (**SI Figure 2D**). The TNP were loaded with a variety of hydrophobic cancer therapeutics, including enzalutamide and the PI3K inhibitor BEZ235, with the rate of release of these compounds by the TNP at pH 6.8 associated with their solubility in DMSO (**SI Figure 2E**).

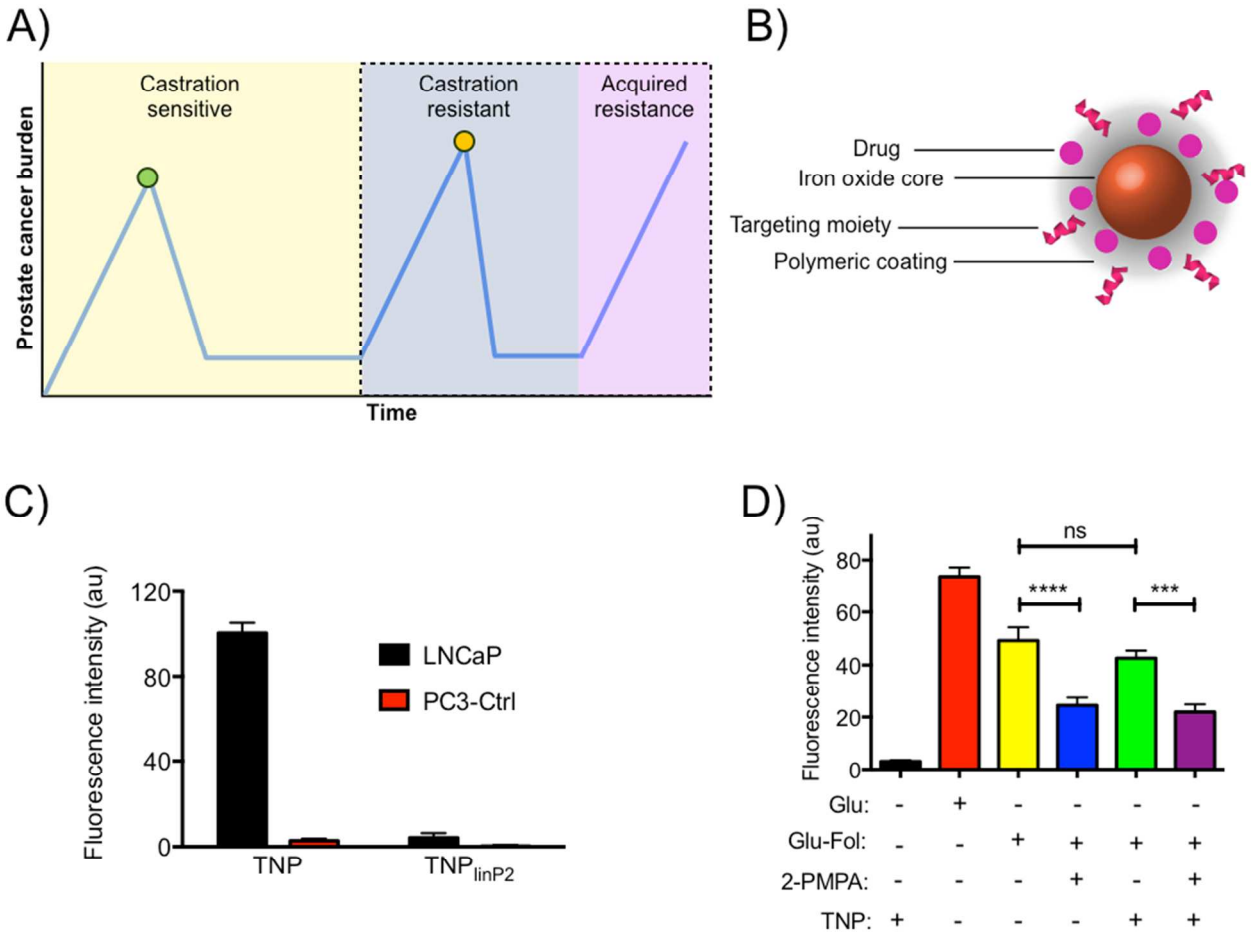

Figure 1. Development of targeted nanopharmaceuticals (TNP) for the recognition of the biomarker FOLH1 (PSMA). (A) Prostate cancer undergoes multiple molecular alterations that give rise to distinct phases. Acquired resistance leads to metastasis, and ultimately to death. (Green circle: hormone deprivation; orange circle: anti-androgens) (B) Schematic representation of the TNP supramolecular architecture. (C) The TNP's cyclic peptide conferred target specificity. Linearization of the peptide (linP2) abrogated binding to PSMA (LNCaP: PSMA-positive cells; PC3-Ctrl: PSMA-negative cells). (D) Binding of the TNP's peptide probe occurred at a locus that did not impair PSMA's enzymatic activity (Glu: glutamic acid; Glu-Fol: monoglutamated folate; 2-PMPA: PSMA inhibitor; ns: not significant; *** $P < 0.001$; **** $P < 0.0001$). Means ± SEM.

Next, we evaluated the specificity of the TNP towards PSMA, utilizing the fluorescence signal of their Cy5.5-modified targeting peptide. The TNP associated with the human prostate cancer cell line LNCaP, which endogenously expresses PSMA, as well as with the human prostate cancer cell line PC3-PSMA, which was engineered to overexpress the TNP's target (**SI**

Figure 3A-B). In the presence of free peptide, the interaction between TNP and PSMA-expressing cells was abrogated, reflected in lower florescence and lack of magnetic resonance (T2) signal (**SI Figure 3A-C**). Intriguingly, we found that although the TNP bound to human PSMA, they did not bind to mouse PSMA, which was overexpressed by genetically engineered CT26-mPSMA cells (**SI Figure 3A inset**). Subsequent bio-distribution studies with radiolabeled TNP (^{89}Zr-TNP) confirmed the *in vitro* findings, and further showed high uptake of the TNP by the human PSMA-expressing tumor PC3-PSMA (**SI Figure 3D**), with nominal retention by the parental human prostate cancer cell line PC3, which lacks PSMA expression. These results demonstrate that the TNP recognize human PSMA with high specificity, and hint to their use as a complimentary PC diagnostic modality.

Towards this direction, we confirmed that the specificity of the TNP is attributed to their targeting peptide's structure, as linearization of the peptide through reduction of its disulfide bridges abrogated binding to PSMA-expressing cells, as well as in the presence of excess concentration of free cyclic peptide (**Figure 1C** and **SI Figures 4A-D**). Since the TNP's targeting moiety binds to PSMA's luminal side, we assessed whether the interaction between the TNP and target cells might be perturbed in the presence of high concentrations of monoglutamate folate (Glu-Fol), which is a natural substrate for PSMA. Results obtained through the Amplex Red glutamate oxidase assay revealed that Glu-Fol did not affect the interaction between TNP and PSMA (**Figure 1D**), suggesting that the TNP associate with PSMA at a location that is distant from the enzyme's active site and that the nanopharmaceutical will not be affected by the presence of endogenous PSMA substrates *in vitro* or *in vivo,* because it carries more robust and selective entities than common targeted therapeutics that bear just folate moieties[21].

Subsequent *in vitro* studies showed that the TNP interacted with PSMA-expressing cells, as reflected in enhanced cell-associated fluorescence and a prominent decrease in the T2 magnetic resonance signal (**Figure 2A**). These findings prompted us to examine whether the TNP could specifically detect PSMA *in vivo*, using male athymic nude mice with human prostate cancer xenografts on their rear flanks (Left: PSMA-negative PC3-Ctrl, Right: PSMA-positive PC3-PSMA). Twenty-four hours post i.v. administration, prominent fluorescence was observed in the PSMA-expressing lesion, as opposed to the PSMA-negative tumor (**Figure 2B**). Similar to

the *in vitro* studies, magnetic resonance imaging showed a lower T2 signal in the tumor expressing the PSMA biomarker (**Figure 2C**), due to specific uptake of the TNP. These imaging results were confirmed with histological analysis which showed enhanced fluorescence attributed to the TNP's Cy5.5 fluorophore and presence of high levels of iron due to the TNP's iron oxide core in the PSMA-positive cells, in contrast to the PSMA-deficient PC3-Ctrl (**Figure 2D**). Taken together, these findings suggest that TNP might be an attractive alternative for the imaging of prostate cancer in the clinic, complementing the emerging radiolabeled small-molecule probes for FOLH1/PSMA[22], without exposing the patients to unnecessary radiation and circumventing their short blood half-life, renal clearance and bladder accumulation.

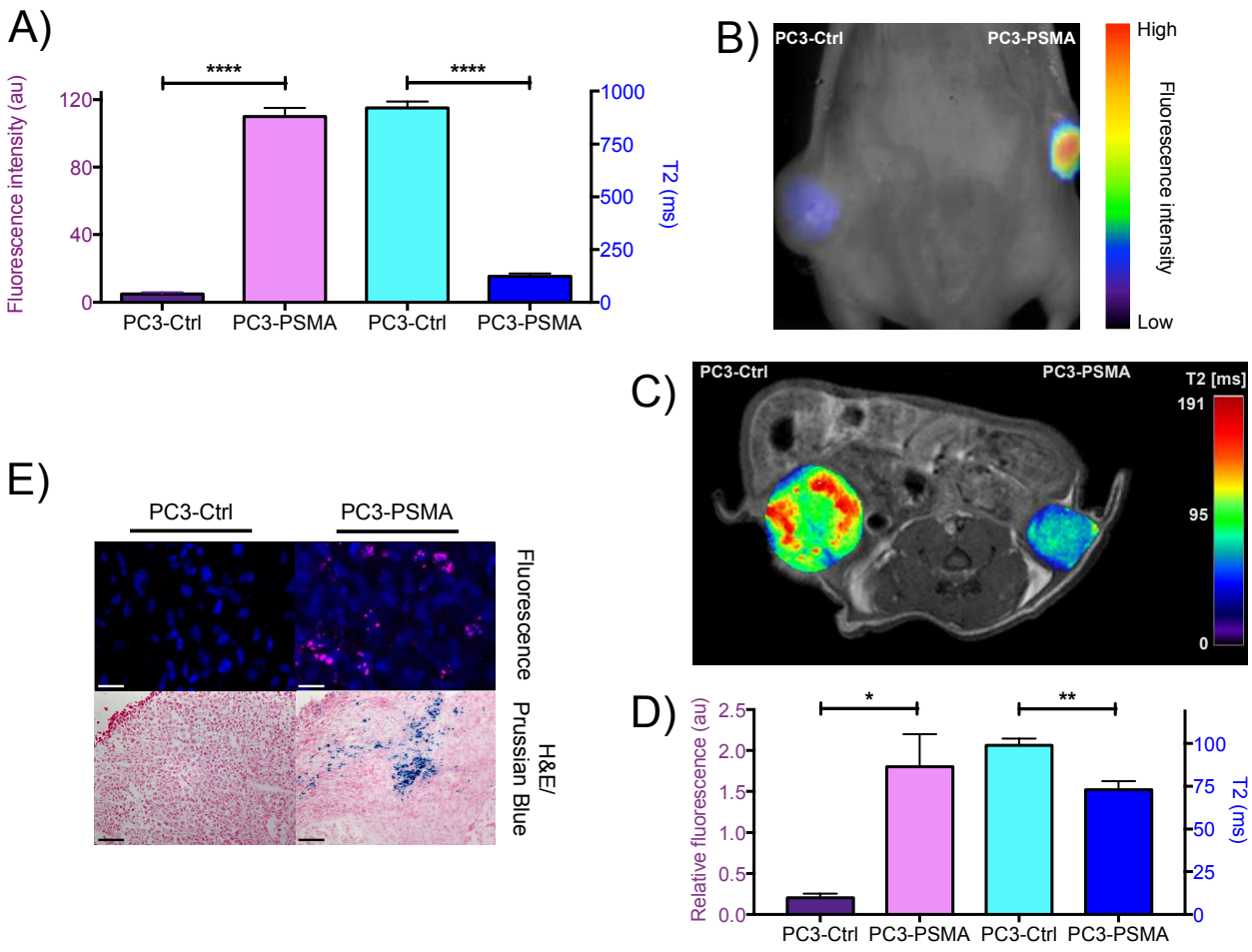

Figure 2. Multimodal biomarker detection with TNP. (A) *In vitro* evaluation of the binding of TNP to plasma-membrane-expressed FOLH1 (PSMA), using the TNP's fluorescence and magnetic resonance signals (PC3-Ctrl: PSMA-negative cells; PC3-PSMA: PSMA-positive cells; **** $P < 0.0001$). (B) Fluorescence tomography showed homing of TNP's to the PSMA-positive tumor in nude, male mice. (C)

Magnetic resonance imaging revealed reduction in the T2 signal of the biomarker-expressing lesion 24 h after iv administration of the TNP. (D) Quantification of fluorescence and magnetic resonance signal due to TNP accumulation in the animals' PSMA-expressing tumors (n=5; * $P < 0.05$, ** $P < 0.01$). (E) Histological analysis of PC3-Ctrl and PC3-PSMA tumors after TNP administration confirmed accumulation of the TNP within the PSMA-positive tumor (blue: Hoechst 333442 nuclear stain; magenta: Cy5.5 dye of TNP; H&E: hematoxylin and eosin stain; Prussian blue: iron stain; Scale $bar_{fluorescence}$: 25 μm; Scare $bar_{H\&E}$: 100 μm). Means ± SEM.

Because the androgen receptor pathway negatively regulates the expression of the *FOLH1* gene[14], we reasoned that the TNP might be able to monitor changes in the signaling of androgen receptor axis through PSMA's levels. For instance, if the androgen receptor were active, such as in the presence of testosterone, PSMA's levels would be down-regulated, whereas upon inhibition of the androgen receptor, such as with an anti-androgen drug, the levels of PSMA would increase. Experiments with the androgen-receptor-expressing LNCaP cells showed that treatment with testosterone or the synthetic androgen R1881 which both activate the androgen receptor pathway decreased the levels of PSMA (**Figure 3A**), whereas enzalutamide treatment that blocks androgen receptor signaling had the opposite effect (**Figure 3B**), in line with prior work[14]. Next, we used TNP for the non-invasive monitoring of response to anti-androgen therapy *in vivo*, utilizing DiR-loaded TNP. Treatment with enzalutamide of animals that had androgen-receptor-expressing xenografts on their flanks caused significant increase of TNP uptake and higher fluorescence, when compared to control animals (**Figures 3C-D**). Hence, this demonstrates that TNP might serve as an affordable, high-throughput platform for the assessment of chemotherapy response in patient-derived xenograft models at the dawn of personalized, precision medicine.

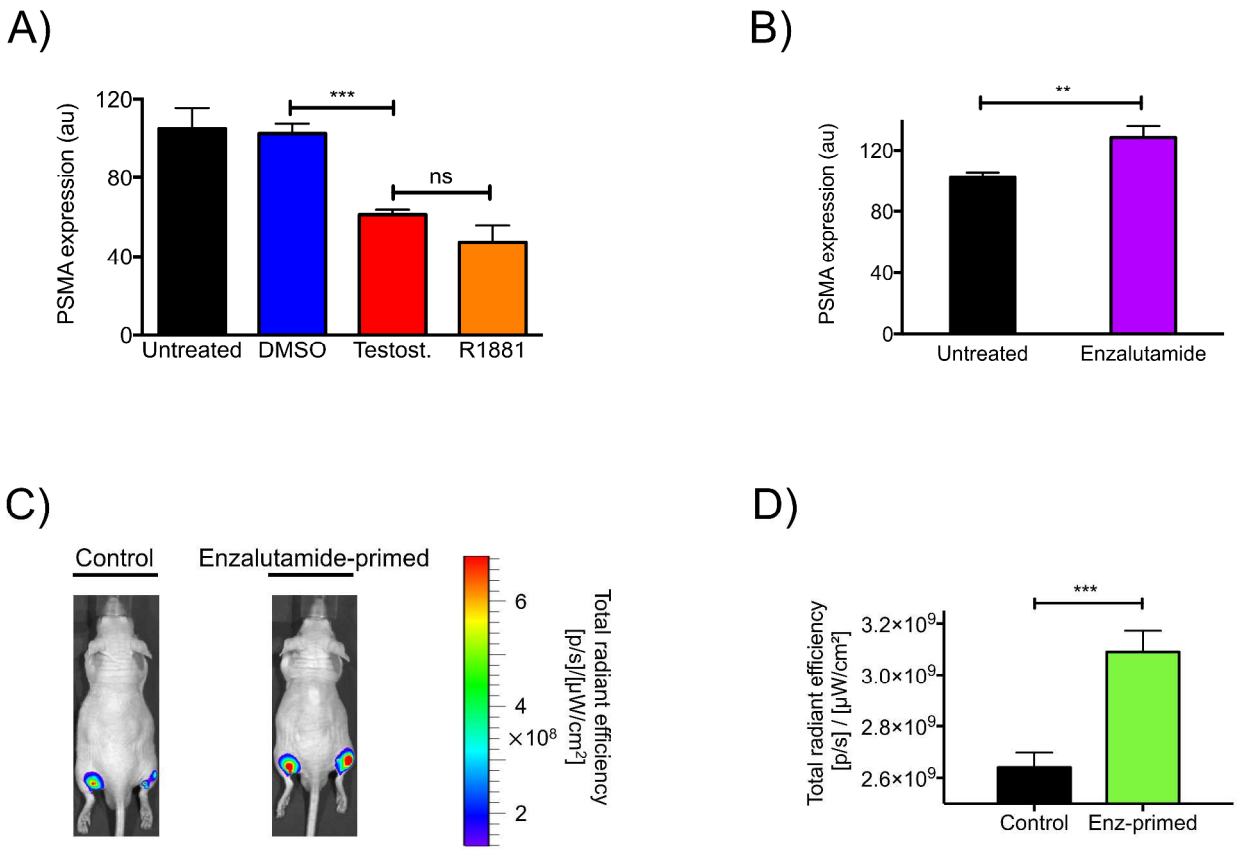

Figure 3. TNP-based evaluation of the androgen receptor pathway in prostate cancer. (A) Treatment with androgens for 96 h decreased the expression of PSMA by LNCaP cells, which assessed with TNP's fluorescence (Testost.: testosterone; R1881: metribolone; ns: not significant; *** $P < 0.001$). (B) Inhibition of androgen receptor signaling for 2 weeks upregulated PSMA expression that resulted more TNP binding (Enzalutamide: Xtandi; ** $P < 0.01$). (C-D) Priming of LNCaP xenografts with enzalutamide caused upregulation of PSMA levels. (Representative images shown. $n_{control} = n_{enz\text{-}primed} = 6$; *** $P < 0.001$). Means ± SEM.

In addition to diagnosis, another critical vignette in cancer treatment is effective delivery of therapy, in order to maximize cancer cell death and prevent resistance. There is an opportunity to exploit the hydrophobic nature of many new chemotherapeutics by loading them to TNP and ensure delivery on target and better bioavailability. Indeed, we were able to load such hydrophobic entities within the polymeric coating of TNP's without subjecting these drugs to any chemical modification. Our results showed that the TNP could cause enhanced cell death in PSMA-expressing cells, due to uptake of the nanopharmaceutical by these cells (**Figure 4A-B**).

Importantly, the drug-loaded TNP were twice more cytotoxic to PSMA-expressing cells than native Ferumoxytol nanoparticles loaded with the same amount of chemotherapeutic (**SI Figure 5A**). The nascent TNP and Ferumoxytol did not cause cell death, as previously observed[8]. Furthermore, PSMA-deficient PC3-Ctrl cells had no difference in cell death induced by either the drug administered in its free form or after treatment with the drug–loaded TNP, indicating that the TNP released their cargo in the acidic extracellular milieu thus causing similar cell death to the free drug (**Figure 4C**). We also confirmed that higher expression of PSMA resulted in higher induction of cell death by drug-loaded TNP (**Figure 4D**), indicating that this nanopharmaceutical has potential to become a translational biomarker-guided delivery platform for FOLH1/PSMA-expressing cancers.

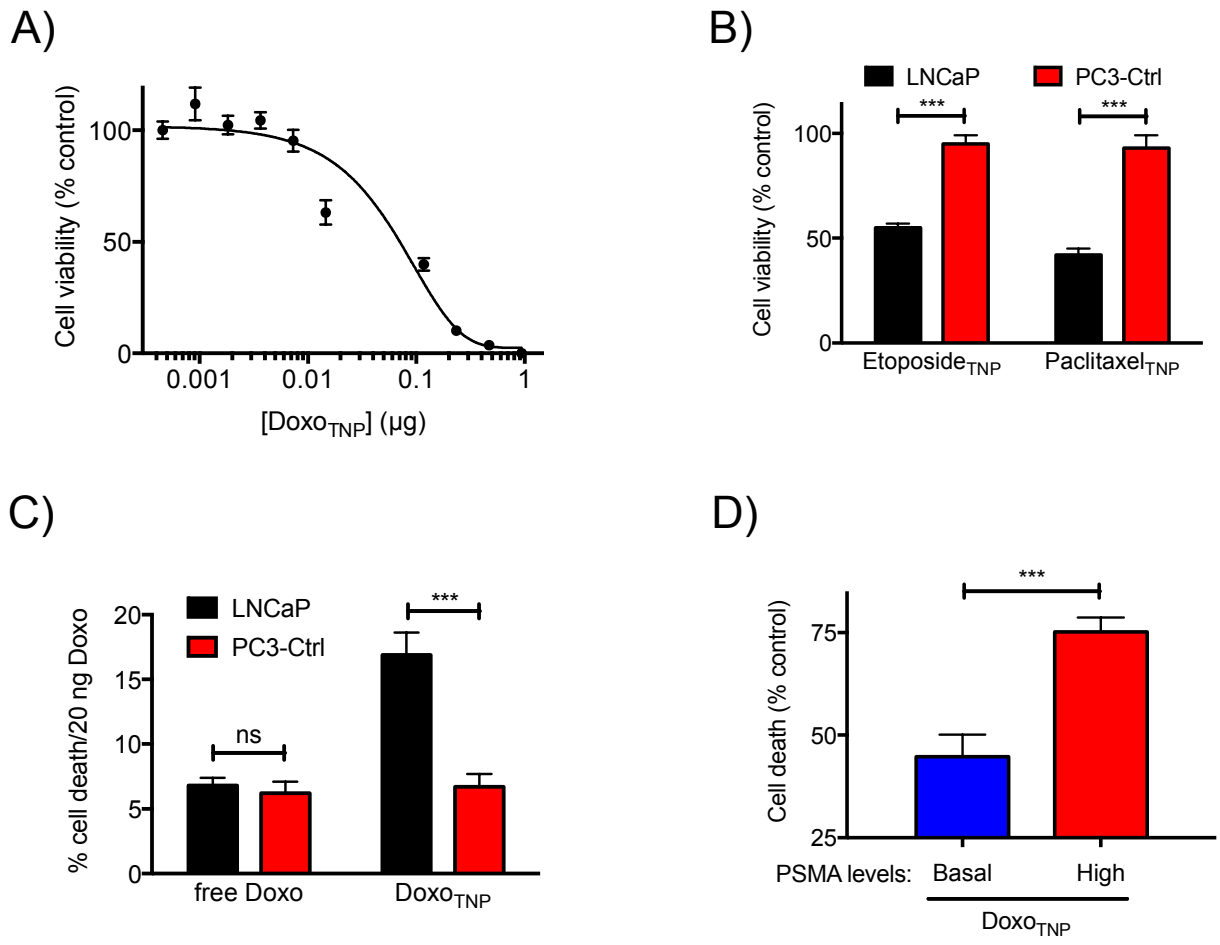

Figure 4. Improved drug delivery with drug-carrying TNP. (A) Delivery of therapy with TNP caused cell death in the PSMA-expressing LNCaP cells (DoxoTNP: doxorubicin-loaded TNP). (B-C) Selective drug delivery of etoposide, paclitaxel and doxorubicin with TNP (LNCaP: FOLH1-positive cells; PC3-Ctrl:

FOLH1-negative cells; *** $P < 0.001$). (D) The levels of PSMA at the plasma membrane of neoplastic cells dictated response to therapy delivered with TNP. Means ± SEM.

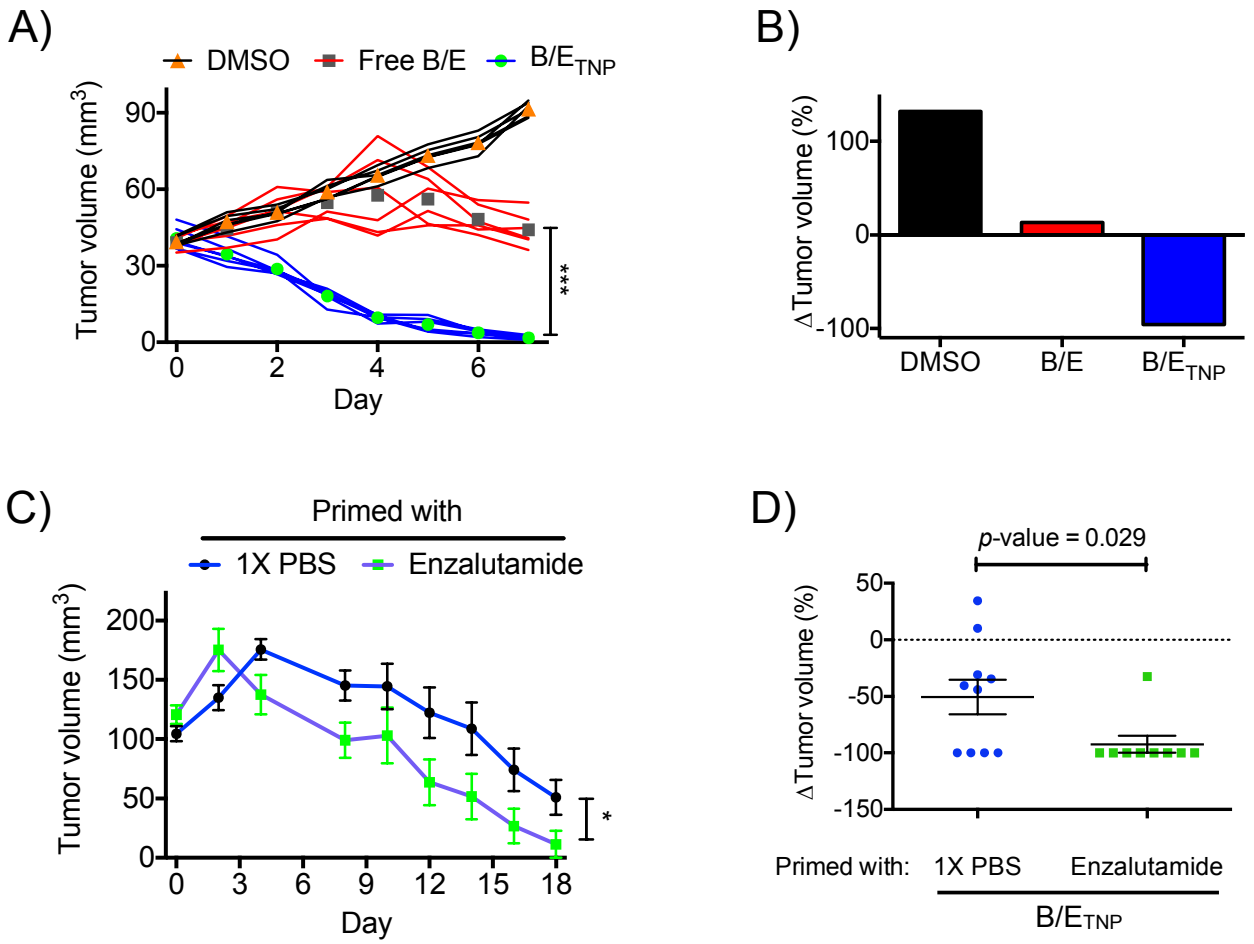

Figure 5. Enhanced tumor response with TNP delivering therapy for castration-resistant disease. (A-B) Co-delivery of the PI3K inhibitor BEZ235 and the anti-androgen enzalutamide achieved tumor regression in athymic, nude male mice with LNCaP xenografts (B: BEZ235; E: enzalutamide; *** $P < 0.001$). (C-D) Priming with enzalutamide prior to treatment with B/E$_{TNP}$ provided improved response and faster regression (* $P < 0.05$). Means ± SEM.

Since combination therapies are needed in order to simultaneously inhibit multiple disease-driving signaling pathways, we co-loaded TNP with enzalutamide and the PI3K inhibitor BEZ235, since in castration-resistant PC both the androgen receptor and PI3K pathways are key drivers of the disease. Intravenous administration of TNP carrying both of these drugs achieved complete tumor regression within a week in animals that had PSMA-expressing, androgen-

receptor-positive xenografts, in the absence of any adverse side effects or loss of weight (**Figure 5A-B**). This was in contrast to animals receiving the therapeutic combination in its free form, where the drugs only yielded a tumor-static effect. Encouraged by these findings, we investigated whether TNP could augment the outcome of monotherapy. Specifically, animals with xenografts that expressed both PSMA and the androgen receptor were treated with either enzalutamide or vehicle (1X PBS) for one week, followed by treatment with enzalutamide/BEZ235-loaded TNP. Results showed faster response and tumor regression in the enzalutamide-primed cohort (**Figure 5C-D**), likely due to early suppression of the androgen receptor pathway and augmentation of therapy as a result of higher TNP uptake facilitated by the transient upregulation of PSMA levels (**Figure 2C-D**). Lastly, we examined whether the TNP could address disease with acquired resistance, which although not responding to anti-androgens and PI3K inhibitors it preserves its PSMA expression in PC patients. As a model *in vivo* system, we used animals with PSMA-positive, androgen-receptor-deficient xenografts, and TNP that were co-loaded with semi-synthetic taxoid cabazitaxel and riluzole, which activates the heat shock transcription factor 1. This protein is over-expressed in human prostate cancer cell lines (**SI Figure 5B**), and many patients with solid malignancies carry amplifications of this gene (**Figure 6A**), making it an attractive therapeutic target, since it was previously shown that activation of this pathway results in cell death through endoplasmic reticulum stress[23, 24]. During a 30-day long study, where treatment was administered iv every other day, co-delivery of cabazitaxel and riluzole with TNP achieved complete tumor regression, whereas TNP loaded only with riluzole had a tumor-static effect and TNP carrying cabazitaxel had no effect on tumor growth (**Figure 6B**). After the end of the treatment phase, we continued monitoring the animals that received combination therapy delivered with TNP, and observed no tumor relapse throughout the end of the study (**Figure 6C**). Collectively, these results show that TNP-based delivery of combination therapies that selectively target focal oncogenic cascades can effectively address disease with acquired resistance, preventing side effects and improving survival.

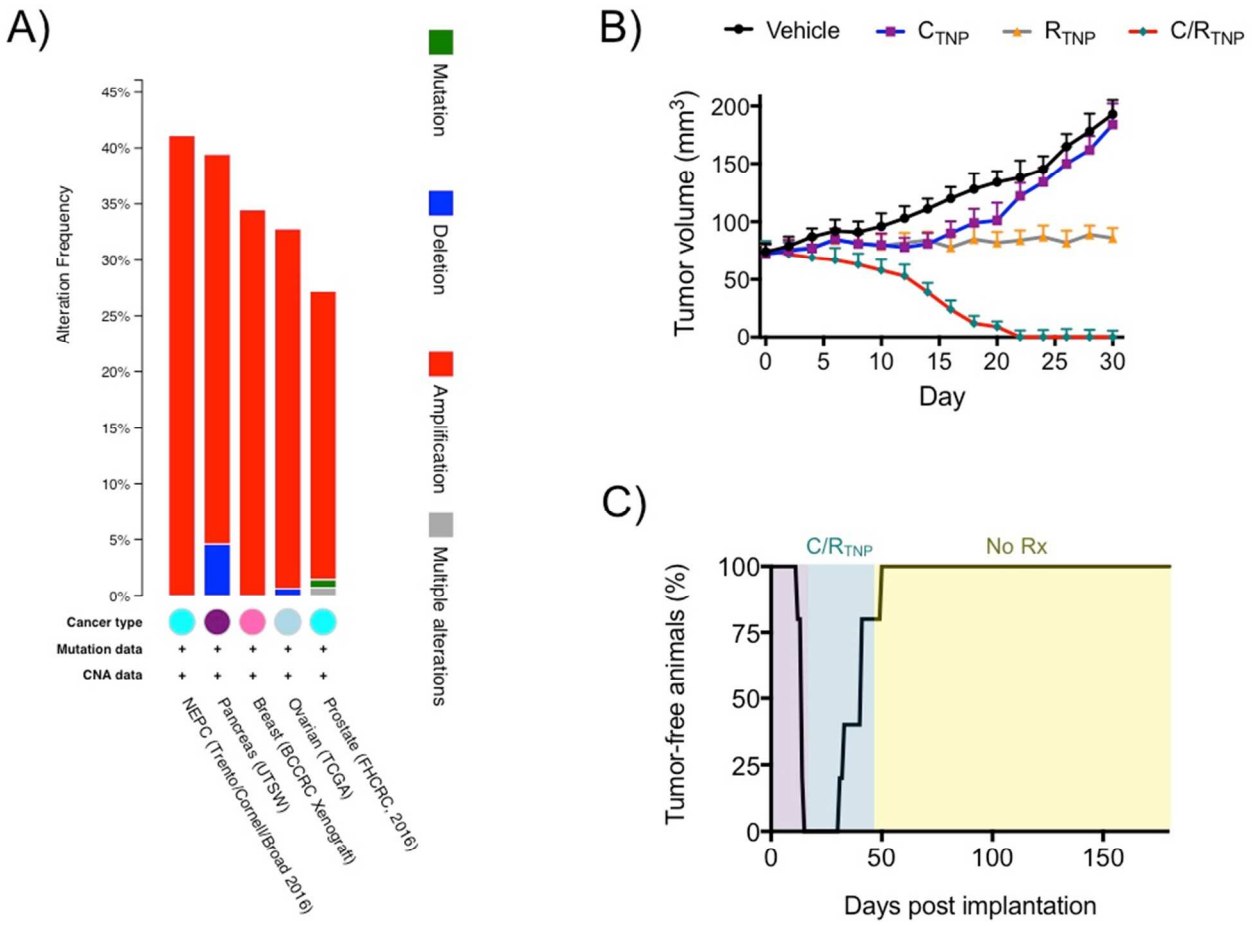

Figure 6. Combination therapy of prostate cancer that has acquired resistance with TNP. (A) The gene encoding the heat-shock transcription factor 1 is amplified in samples from cancer patients. (B) Simultaneous delivery of riluzole, which increases the steady-state levels of the heat-shock transcription factor 1, and cabazitaxel with TNP resulted in tumor regression, and (C) robust response with no relapse. Means ± SEM.

Overall, we demonstrated that TNP could be used for precision medicine using the levels of the biomarker PSMA as a molecular inflection point that guided treatment. We also showed how these inflection points could be used to deliver effective therapies that selectively target molecular drivers of distinct disease phases. Because the TNP retain their cargo via weak electrostatic forces, it is anticipated that different drugs can be loaded within these nanopharmaceutical carriers for mono- or combination therapies for prostate cancer or other solid tumors, whose neovasculature expresses PSMA. Furthermore, with the rise of genomics and proteomics, other inflection points might be identified, as well as novel therapeutic targets,

which can be inhibited with small molecules carried by the TNP. From a clinical standpoint, this nanopharmaceutical platform allows sensitive diagnosis with a clinically relevant agent, and treatment with the very same agent that was used for imaging. Apart from oncology, we believe that applications based on TNP may span other disease areas, including inflammation and neurodegeneration, where imaging holds the premise to guide personalized therapy. At the dawn of precision medicine, the TNP may lower disease mortality, support a healthier society, and lower treatment costs, using new molecular insights from multiple disciplines harnessed through nanotechnology.

Materials and Methods

Chemicals. Dimethyl sulfoxide (DMSO), folate monoglutamate (Glu-Fol), glutamic acid, Tris(2-carboxyethyl)phosphine hydrochloride (TCEP), 2-PMPA, R1881 and testosterone were obtained from Sigma Aldrich (Saint Louis, MO). Doxorubicin, etoposide, paclitaxel, cabazitaxel, enzalutamide, BEZ235, and riluzole were purchased from Selleck Chemicals (Houston, TX). DiR was procured from Life Technologies (Carlsbad, CA), 89-zirconium oxalate from 3D Imaging, LLC (Maumelle, AR), whereas the MSKCC Chemistry Core provided us with the cyclized unlabeled and Cy5.5-modified PSMA-specific peptides, which were synthesized as previously reported[20]. Ferumoxytol was obtained from AMAG Pharmaceuticals (Lexington, MA).

Cell lines. LNCaP and PC3 cells were obtained from ATCC (Manassas, VA), and maintained according to the supplier's instructions. The cell lines PC3-PSMA and CT26-mPSMA were provided by Dr. Vladimir Ponomarev (MSKCC). All cell lines were authenticated by DDC Medical (Fairfield, OH), which confirmed the cell lines' identity.

Animal Models. The animals were obtained from Harlan Laboratories (currently Envigo, Somerset, NJ), and all animal studies were done in accordance with protocols approved by the Institutional Animal Care and Use Committee of Memorial Sloan Kettering Cancer Center, following the National Institutes of Health guidelines for animal welfare.

Nanopharmaceutical formulation. Conjugation of the cyclical disulfide-containing PSMA-specific peptide was achieved through EDC-based chemistry as previously described[25], followed by dialysis to remove any free peptide that did not conjugate to the nanoparticles. Through

UV/Vis and fluorescence spectroscopy, it was determined that on average there were 12 Cy5.5-labeled peptides on each nanoparticle. Encapsulation of either DiR or drugs was achieved using the solvent-diffusion method[8], which facilitated entrapment of the hydrophobic cargo within the carboxymethyl dextran coating. Briefly, 30 μL of Ferumoxytol were resuspended in 500 μL distilled water, and the cargo was diluted to 100 μL DMSO at the desired concentration. The DMSO solution was added dropwise to the nanoparticle solution under continuous vortexing at 1,000 r.p.m at room temperature. The resulting formulations were then dialyzed using a dialysis chamber (MWCO 3,000, Fisher) against 1× PBS, followed by storage at 4 ^{o}C.

Characterization of nanopharmaceuticals. The size of the nanoparticles was determined through dynamic light scattering (Nano-ZS, Malvern, Westborough, MA), and the same instrument was used to measure the surface charge (ζ potential). The iron concentration of the formulations was determined spectrophotometrically as previously reported[26], using a SpectraMax M5 instrument (Molecular Devices, Sunnyvale, CA). In summary, we digested the nanoparticles in acid, and then converted all iron ions to Fe^{+3}. A standard curve was created based on the absorbance at 410 nm of solutions of known concentration of $FeCl_3$ in the digesting solution. Fluorescence emission measurements were performed using the SpectraMax M5, as well as an Odyssey near-infrared imaging station (LI-COR Biosciences, Lincoln, NE), equipped with two solid-state lasers for excitation at 685 and 785 nm. The molar extinction coefficients of Doxorubicin (11,500 $M^{-1}cm^{-1}$ at 480 nm) and DiR (270,000 $M^{-1}cm^{-1}$ at 748 nm) were utilized, in order to determine the nanopharmaceutical's cargo content. For the rest of the drugs, we quantified the amount of drug-loaded into the nanoparticles using HPLC and standard curves with known amounts of the corresponding drug. To achieve this, we triggered release of the cargo by incubating the loaded nanoparticles in a 2M NaCl solution for 30 min, followed by spin filtration (MWCO 5000) to collect the cargo-containing solution. Through this approach, we determined that the TNPs' loading efficiency was: 78 ± 5% for Doxorubicin, 69 ± 3% for DiR, 42 ± 6% for etoposide, 38 ± 4% for paclitaxel, 53 ± 2% for enzalutamide, 58 ± 6% for BEZ235, 61 ± 5 % for cabazitaxel and 29 ± 4% for riluzole. Stability experiments were performed in pH-adjusted PBS, whereas serum experiments were performed at 37 °C, using fetal bovine serum obtained from Gemini Bio-products. The release of drugs at different pH was determined with a dynamic dialysis setup, according to a previous report[27]. A dialysis chamber was utilized (MWCO 3000, Fisher), containing the drug-loaded nanopharmaceutical at the indicated pH-

adjusted 1× PBS, with the nanoparticles dialyzed against the corresponding pH-adjusted buffer at room temperature and under constant stirring (150 r.p.m.). At regular time points, aliquots from the external aqueous milieu of the device were collected for further analysis. The collected samples were analyzed via a Beckman Coulter HPLC instrument, equipped with a C18 reverse phase column and UV/Vis detector.

Evaluation of the interaction between the targeted nanopharmaceutical and PSMA-expressing cells. In order to determine the association of the TNP with cells, we used the human prostate cancer cell lines LNCaP (PSMA-positive) and PC3-Ctrl (PSMA-negative), as well as the mouse colon cancer cell line CT26 that expressed mouse PSMA, which were seeded on a 96-well plate at a density of 6,000 cells per well. After 48 h of adherence and growth at 37^{o}C, 5% CO_2, the cells were treated with TNP carrying the cyclized Cy5.5-labeled peptide or the linearized fluorescent peptide, which was treated with TCEP prior to conjugation to the nanoparticles. After 3 h at 37 ^{o}C, 5% CO_2, the cells were washed three times with warm PBS, and their fluorescence was evaluated with the SpectraMax M5 instrument, quantifying the Cy5.5 emission signal. The same approach was utilized for the evaluation of cargo with the TNP ([Fe] = 5 μg/mL). In this experiment, the non-fluorescent peptide was conjugated to the nanoparticles, which were then loaded with the hydrophobic dye DiR. Assessment of the interaction of TNP with PSMA-expressing cells in solution via magnetic relaxation was performed using a competition assay format[28] that utilized the free unmodified cyclic peptide and LNCaP cells resuspended in 1× PBS (25,000 cells per 200 μL). Changes in the relaxation signal were measured with a benchtop relaxometer operating at 0.47T (MiniSpec, Bruker, Billerica, MA). We used the Amplex Red Glutamic Acid assay (Thermo Fisher) to determine whether the TNP carrying the cyclized peptide interacted with PSMA at a site other than its catalytic pocket. The assay was performed according to the supplier's guidelines, and in the presence of LNCaP cells (25,000 cells per 100 μL), which were added to the reaction solution as the source of plasma-membrane-bound PSMA. The sample conditions included monoglutamated folate (100 nM), 2-PMPA (10 nM), glutamic acid (100 nM), or TNP ([Fe] = 2 μg/mL). In order to determine the association of the TNP with PSMA-expressing tumors, we contacted studies with adult male, athymic, nude mice, bearing PC3-Ctrl and PC3-PSMA xenografts on each flank (n = 5 animals). For each xenograft implantation, 1,000,000 cells in 100 μL in Matrigel (Corning, Fisher

Scientific) were injected subcutaneously. After tumor formation, 50 μCi of ^{89}Zr-labeled TNP ([Fe] = 1 mg/mL, 200 μL), which was prepared using a chelator-free heat-assisted radiolabeling approach[29], were administered i.v., followed by euthanasia and organ collection 24 h post administration. The radioactivity of the organs was measured with a PerkinElmer Wizard^2 2480 Automatic Gamma Counter (Waltham, MA).

***In vivo* imaging and therapy studies.** *In vitro* optimization studies aimed at detecting PSMA-expressing cells in solution, where LNCaP (PSMA-positive) or PC3-Ctrl (PSMA-negative) cells were incubated with the TNP that were conjugated with the Cy5.5-labeled peptide. Specifically, 100,000 cells in 200 μL 1× PBS were incubated with TNP ([Fe] = 5 μg/mL) for 30 min under continuous vortexing at room temperature. Then, the cells were centrifuged at 1,200 rpm for 5 min, with the resulting cell pellets resuspended in 200 μL 1× PBS, and the whole process repeated three times. Following the final resuspension, the samples' fluorescence and magnetic resonance signal (T2) were measured using the SpectraMax M5 and MiniSpec instruments, respectively. For *in vivo* imaging studies, we used athymic male nude mice with human prostate cancer xenografts on their flanks, which were derived from the PC3-Ctrl (PSMA-negative) and PC3-PSMA (PSMA-positive) cell lines, and implanted as described above. Twenty-four hours after iv administration of the multimodal TNP (fluorescence probe: Cy5.5-carrying PSMA peptide conjugated to the nanoparticles, [Fe] = 1 mg/mL, 200 μL), the animals were imaged using the Maestro fluorescence-based in vivo imaging system (CRi, Woburn, MA; acquired by Perkin Elmer), and a 4.7 T Bruker Biospin MRI using a 35-mm radiofrequency coil. In order to evaluate whether the TNP could report changes due to molecular therapy in cancer, the androgen-receptor-expressing human prostate cancer cell line LNCaP was used, which also expressed PSMA at the cell's plasma membrane. For treatment with testosterone and R1881, the cells were seeded on black-walled, clear-bottom 96-well plates at a density of 5,000 cells per well, supplemented with 100 μL 10% FBS-containing RPMI medium. The cells were then treated as previously described[14], with controls including cells incubated with DMSO corresponding to the drug's final solvent concentration. After 96 h, the cells were washed three times with PBS, and incubated for 30-min with the Cy5.5-labeled TNP ([Fe] = 5 μg/mL) at room temperature, under rocking. The cells were then washed three times with PBS, and evaluation of fluorescence was done with the SpectraMax plate reader. For determination of response to anti-

androgen therapy, we seeded 2,5000 cells per well, and treated them according to a prior report[14]. Following the methodology of that study, *in vivo* evaluation of response to anti-androgen therapy was done with mice that had LNCaP xenografts on their flanks, and were imaged with the IVIS Spectrum (PerkinElmer) system 2 weeks after initiation of anti-androgen therapy, using the DiR-loaded TNP (24 h post iv administration, [Fe] = 1 mg/mL, 200 μL). To evaluate the drug-loaded TNPs toxicity profile, LNCaP cells were seeded at a density of 10,000 cells per well on black-walled, clear-bottom 96-well plates, with 100 μL 10% FBS-containing RPMI medium. PC3-Ctrl cells were grown in 10% FBS-containing F12K medium. Dose-response curves were obtained after the cells were treated for 48 h with corresponding agent. Subsequently, the old medium was aspirated, and cell viability was assessed via the Alamar Blue method (Life Technologies, Carlsbad, CA). The cells were supplemented with 10% Alamar blue-containing medium (10% FBS-containing RPMI or F12K), followed by 3-h incubation in a humidified incubator (37 °C, 5% CO_2) and fluorescence emission was recorded (λ_{exc} = 565 nm, λ_{em} = 585 nm) with the SpectraMax M5 plate reader. Cell viability studies with either etoposide- or paclitaxel-loaded TNP were done at a final iron concentration of 5 μg/mL. Augmentation of therapy due to PSMA overexpression due to pre-treatment with anti-androgen was conducted 2 weeks post treatment with enzalutamide as described above, followed by incubation with the doxorubicin-loaded TNP for 48 h ([Fe] = 5 μg/mL), and assessment of cell viability using the aforementioned Alamar Blue method. Evaluation of the TNPs therapeutic potential in animals was done using adult, male, nude mice (n = 5 per treatment group), which had bilateral LNCaP tumors on their flanks. The animals received i.v. administration of the treatment on days 0, 2, 4 and 6 with 100 μL of equimolar ([BEZ235] = 250 μM, [enzalutamide] = 100 μM) concentrations of either free drugs (diluted in 5% DMSO-containing 1X PBS) or dual-drug-loaded TNP. Control animals were treated with 5% DMSO-containing 1X PBS, and tumor volume was measured with calipers. Priming with enzalutamide for one week was done as previously described[14], which was followed by treatment with the BEZ235/enzalutamide-loaded TNP administered every other day at the levels described above. For the prostate cancer model with acquired resistance, we used adult, male, nude mice (n = 5 per treatment group), which had bilateral PC3-PSMA (PSMA positive, AR negative) tumors on their flanks. During the course of a month, the animals received treatment every other day, which consisted of either monotherapy or combination therapy delivered via the TNP ([cabazitaxel] = 200 μM, [riluzole] = 80 μM).

Data Analysis. All experiments were performed in triplicate unless otherwise stated, with the results presented as mean ± s.e.m. The data were analyzed in Prism (GraphPad Software), whereas the MR images were processed through the OsiriX DICOM viewer.

ASSOCIATED CONTENT

Supporting Information. Molecular modeling, physical characterization of the nanoparticles, drug release, quantification of nanoparticle avidity to PSMA, in vitro studies assessing nanoparticle specificity, and HSF1 levels in prostate cancer cell lines. This material is available free of charge via the Internet at http://pubs.acs.org.

AUTHOR INFORMATION

Corresponding Author

*Address correspondence to grimmj@mskcc.org.

ACKNOWLEDGMENT

This study was supported by the Prostate Cancer Foundation, Alex's Lemonade Stand Foundation, and NIH fund R01 EB017699 (all to C.K.) This research was also partially supported by Mr. William H. and Mrs. Alice Goodwin, the Commonwealth Foundation for Cancer Research, the Center for Experimental Therapeutics of Memorial Sloan Kettering Cancer Center, the Center of Molecular Imaging and Nanotechnology, the Department of Defense, and the NIH fund 1R01CA183953-01A1 (all to J.G.). The authors thank the staff of the MSKCC animal MRI core for providing expert technical assistance. Technical services provided by the MSKCC Small Animal Imaging Core Facility, and the Organic Synthesis Core Facility were

supported in part by the MSKCC NIH Core Grant (P30-CA008748) and NIH Shared Instrumentation Grant No 1 S10 OD016207-01. Dr. George Sukenick and Ms. Hui Fang of the MSKCC NMR Analytical Core are thanked for help with mass spectrometry and NMR.

REFERENCES

1. Kiessling, F.; Mertens, M. E.; Grimm, J.; Lammers, T. *Radiology* **2014,** 273, (1), 10-28.
2. Scheinberg, D. A.; Grimm, J.; Heller, D. A.; Stater, E. P.; Bradbury, M.; McDevitt, M. R. *Curr. Opin. Biotechnol.* **2017,** 46, 66-73.
3. Weissleder, R.; Schwaiger, M. C.; Gambhir, S. S.; Hricak, H. *Sci. Transl. Med.* **2016,** 8, (355), 355ps16.
4. Kaittanis, C.; Shaffer, T. M.; Thorek, D. L.; Grimm, J. *Crit. Rev. Oncog.* **2014,** 19, (3-4), 143-76.
5. Lee, M. J.; Ye, A. S.; Gardino, A. K.; Heijink, A. M.; Sorger, P. K.; MacBeath, G.; Yaffe, M. B. *Cell* **2012,** 149, (4), 780-94.
6. Liu, S.; Kurzrock, R. *Cancer Treat. Rev.* **2014,** 40, (7), 883-91.
7. Liu, S.; Kurzrock, R. *Semin. Oncol.* **2015,** 42, (6), 863-75.
8. Kaittanis, C.; Shaffer, T. M.; Ogirala, A.; Santra, S.; Perez, J. M.; Chiosis, G.; Li, Y.; Josephson, L.; Grimm, J. *Nat. Commun.* **2014,** 5, 3384.
9. Kaittanis, C.; Shaffer, T. M.; Bolaender, A.; Appelbaum, Z.; Appelbaum, J.; Chiosis, G.; Grimm, J. *Nano Lett.* **2015,** 15, (12), 8032-43.
10. Carver, B. S.; Chapinski, C.; Wongvipat, J.; Hieronymus, H.; Chen, Y.; Chandarlapaty, S.; Arora, V. K.; Le, C.; Koutcher, J.; Scher, H.; Scardino, P. T.; Rosen, N.; Sawyers, C. L. *Cancer Cell* **2011,** 19, (5), 575-86.
11. Schwartz, S.; Wongvipat, J.; Trigwell, C. B.; Hancox, U.; Carver, B. S.; Rodrik-Outmezguine, V.; Will, M.; Yellen, P.; de Stanchina, E.; Baselga, J.; Scher, H. I.; Barry, S. T.; Sawyers, C. L.; Chandarlapaty, S.; Rosen, N. *Cancer Cell* **2015,** 27, (1), 109-22.
12. Rajasekaran, A. K.; Anilkumar, G.; Christiansen, J. J. *Am. J. Physiol.* **2005,** 288, (5), C975-81.
13. Ristau, B. T.; O'Keefe, D. S.; Bacich, D. J. *Urol. Oncol.* **2014,** 32, (3), 272-9.
14. Evans, M. J.; Smith-Jones, P. M.; Wongvipat, J.; Navarro, V.; Kim, S.; Bander, N. H.; Larson, S. M.; Sawyers, C. L. *Proc. Natl. Acad. Sci. U. S. A.* **2011,** 108, (23), 9578-82.
15. Perner, S.; Hofer, M. D.; Kim, R.; Shah, R. B.; Li, H.; Moller, P.; Hautmann, R. E.; Gschwend, J. E.; Kuefer, R.; Rubin, M. A. *Hum. Pathol.* **2007,** 38, (5), 696-701.
16. Ross, J. S.; Sheehan, C. E.; Fisher, H. A.; Kaufman, R. P., Jr.; Kaur, P.; Gray, K.; Webb, I.; Gray, G. S.; Mosher, R.; Kallakury, B. V. *Clin. Cancer Res.* **2003,** 9, (17), 6357-62.
17. Minner, S.; Wittmer, C.; Graefen, M.; Salomon, G.; Steuber, T.; Haese, A.; Huland, H.; Bokemeyer, C.; Yekebas, E.; Dierlamm, J.; Balabanov, S.; Kilic, E.; Wilczak, W.; Simon, R.; Sauter, G.; Schlomm, T. *The Prostate* **2011,** 71, (3), 281-8.
18. Ferte, C.; Andre, F.; Soria, J. C. *Nat. Rev. Clin. Oncol.* **2010,** 7, (7), 367-80.
19. Watson, P. A.; Arora, V. K.; Sawyers, C. L. *Nat. Rev. Cancer* **2015,** 15, (12), 701-11.
20. Lupold, S. E.; Rodriguez, R. *Mol. Cancer Ther.* **2004,** 3, (5), 597-603.
21. Flores, O. S., S.; Kaittanis, C.; Bassiouni, R.; Khaled, A. S.; Khaled, A. R.; Perez, J. M. *Theranostics* **2017,** 7, (9), 2477-2494.

22. Eder, M.; Schafer, M.; Bauder-Wust, U.; Hull, W. E.; Wangler, C.; Mier, W.; Haberkorn, U.; Eisenhut, M. *Bioconjugate Chem.* **2012,** 23, (4), 688-97.
23. Akamatsu, K.; Shibata, M. A.; Ito, Y.; Sohma, Y.; Azuma, H.; Otsuki, Y. *Anticancer Res.* **2009,** 29, (6), 2195-204.
24. O'Callaghan-Sunol, C.; Sherman, M. Y. *Cell Cycle* **2006,** 5, (13), 1431-7.
25. Yuan, H.; Wilks, M. Q.; El Fakhri, G.; Normandin, M. D.; Kaittanis, C.; Josephson, L. *PloS One* **2017,** 12, (2), e0172722.
26. Nath, S.; Kaittanis, C.; Ramachandran, V.; Dalal, N.; Perez, J. M. *Chem. Mater.* **2009,** 21, (8), 1761-1767.
27. Santra, S.; Kaittanis, C.; Perez, J. M. *Langmuir* **2010,** 26, (8), 5364-73.
28. Santiesteban, O. J.; Kaittanis, C.; Perez, J. M. *Angew. Chem.* **2012,** 51, (27), 6728-
29. Boros, E.; Bowen, A. M.; Josephson, L.; Vasdev, N.; Holland, J. P. *Chem. Sci.* **2015,** 6, (1), 225-236.

Table of Contents Graphic.

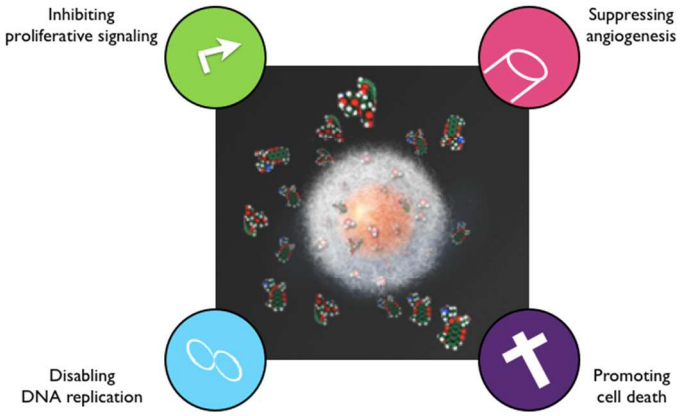

A)

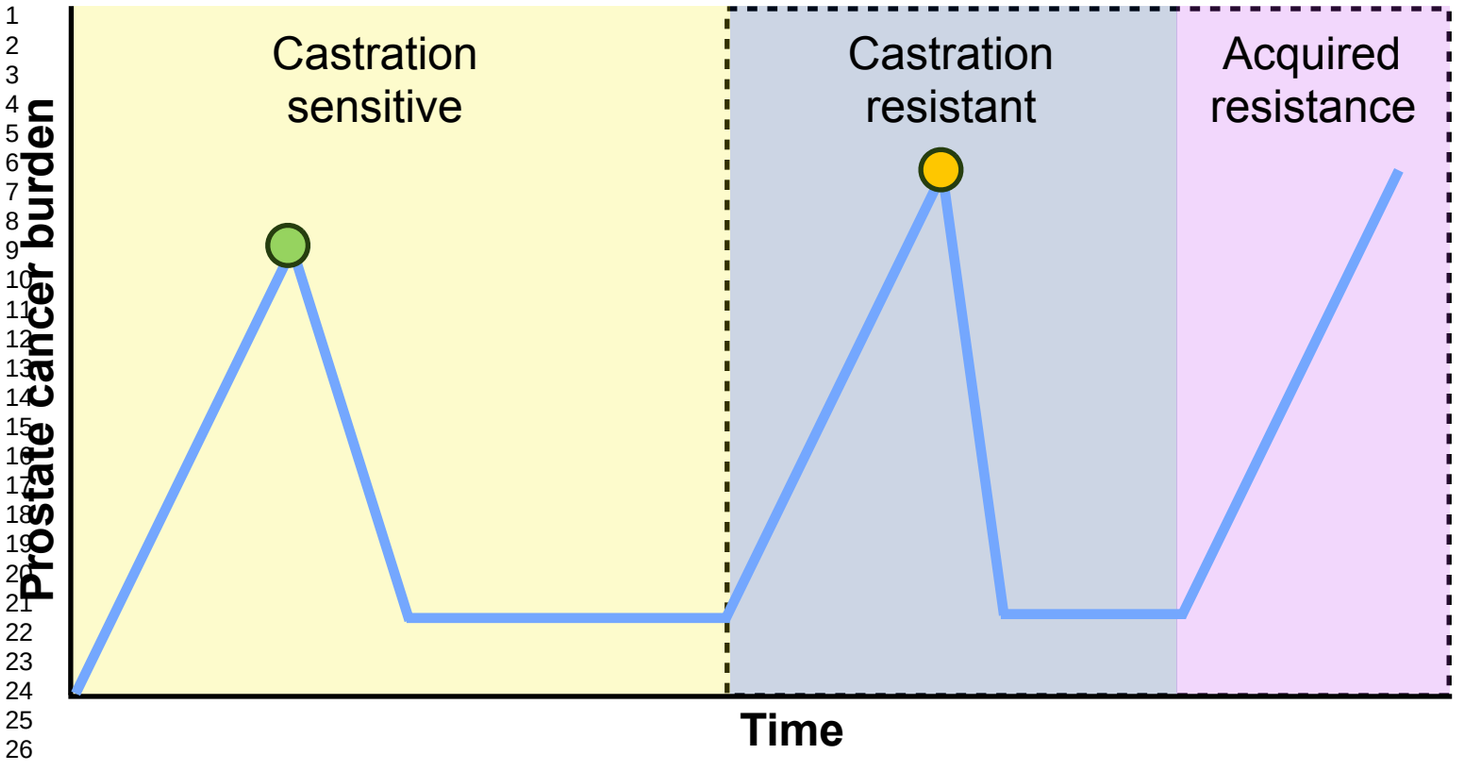
Castration sensitive
Castration resistant
Acquired resistance
Prostate cancer burden
Time

B)

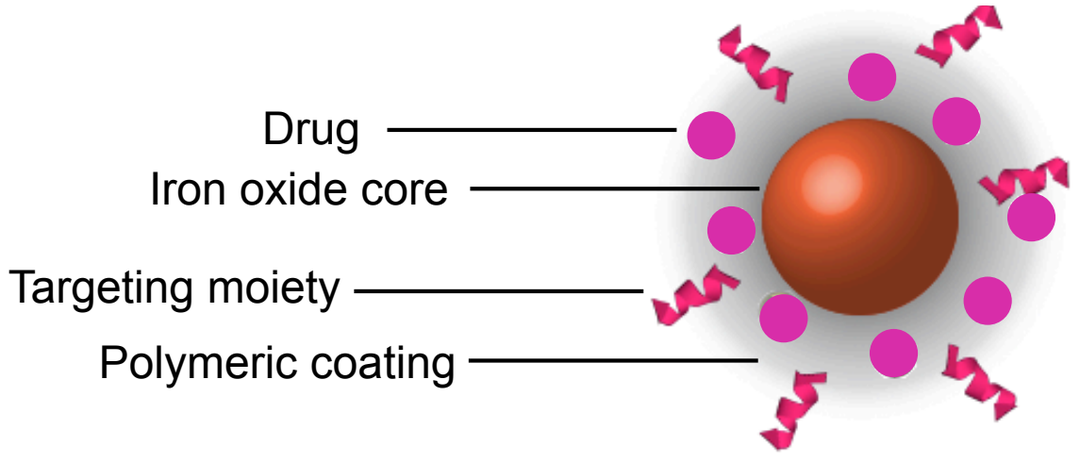
Drug
Iron oxide core
Targeting moiety
Polymeric coating

C)

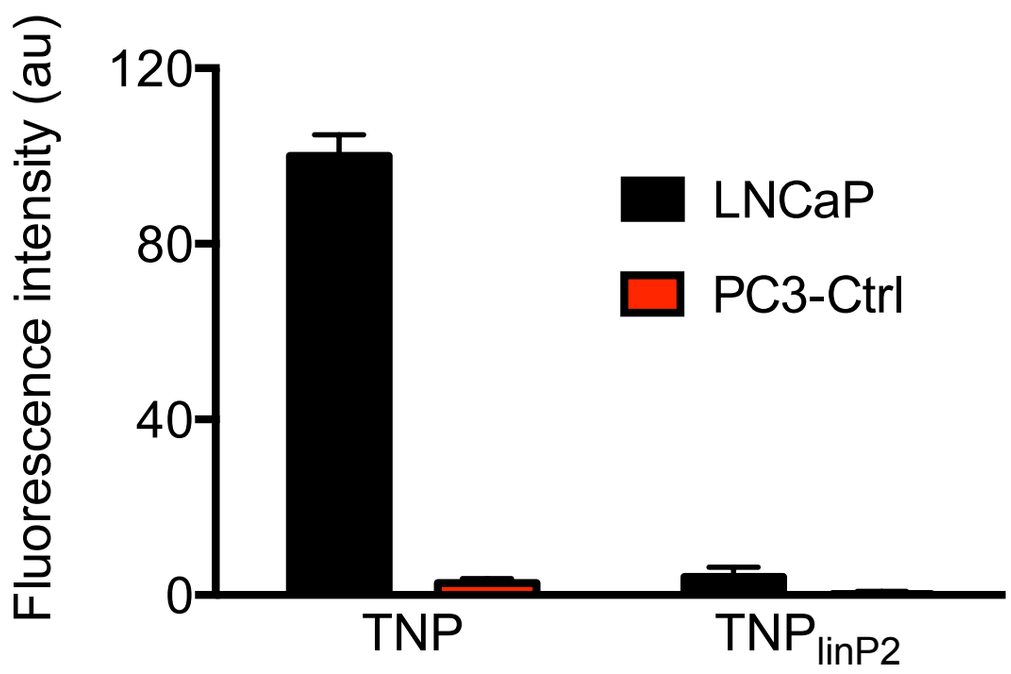
Fluorescence intensity (au)
120
80
40
0
LNCaP
PC3-Ctrl
TNP
TNP linP2

D)

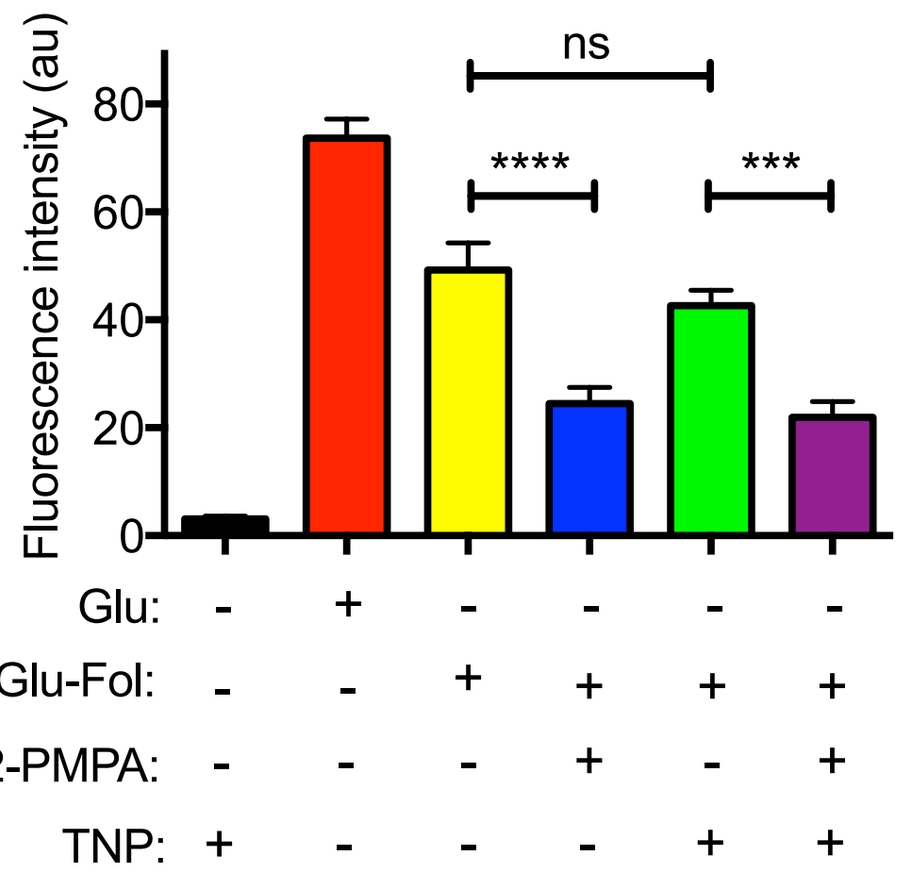
Fluorescence intensity (au)
80
60
40
20
0
ns
****
***
Glu: - + - - - -
Glu-Fol: - - + + + +
2-PMPA: - - - + - +
TNP: + - - - + +

A)

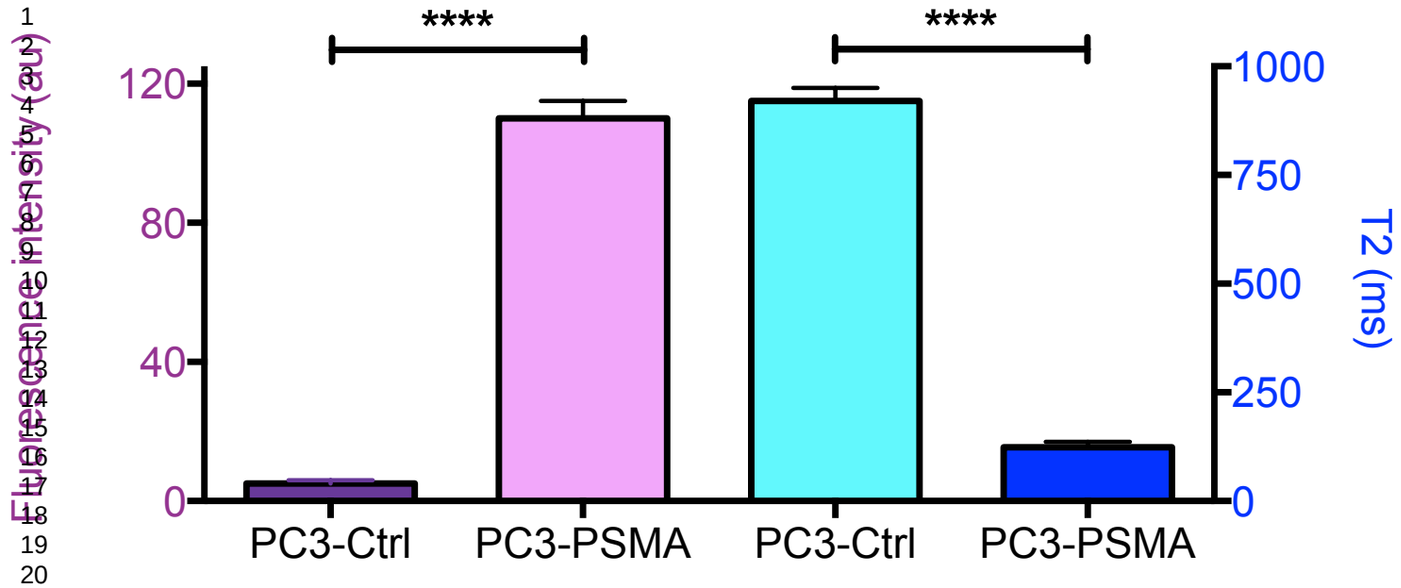
****
****
120
80
40
0
1000
750
500
250
0
Fluorescence intensity (au)
T2 (ms)
PC3-Ctrl
PC3-PSMA
PC3-Ctrl
PC3-PSMA

B)

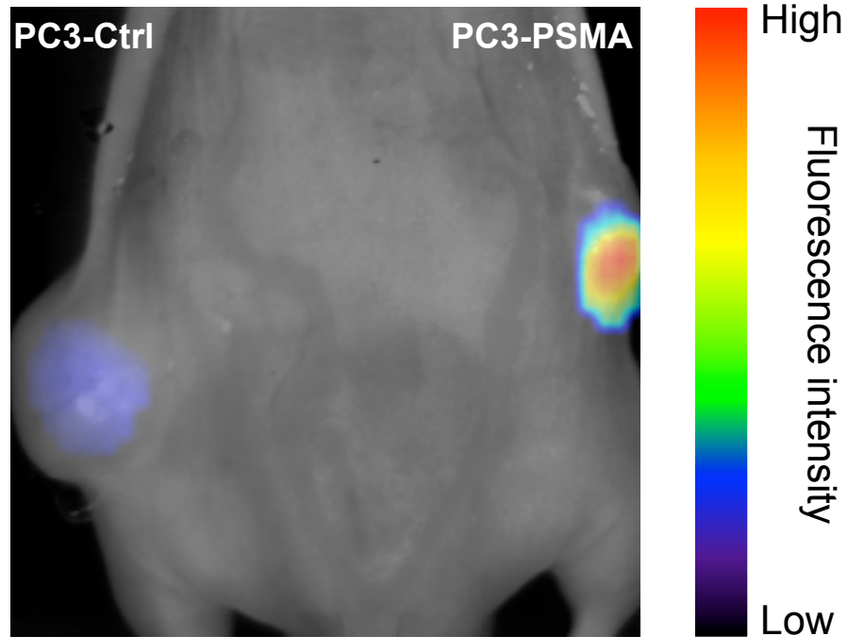
PC3-Ctrl
PC3-PSMA
High
Fluorescence intensity
Low

C)

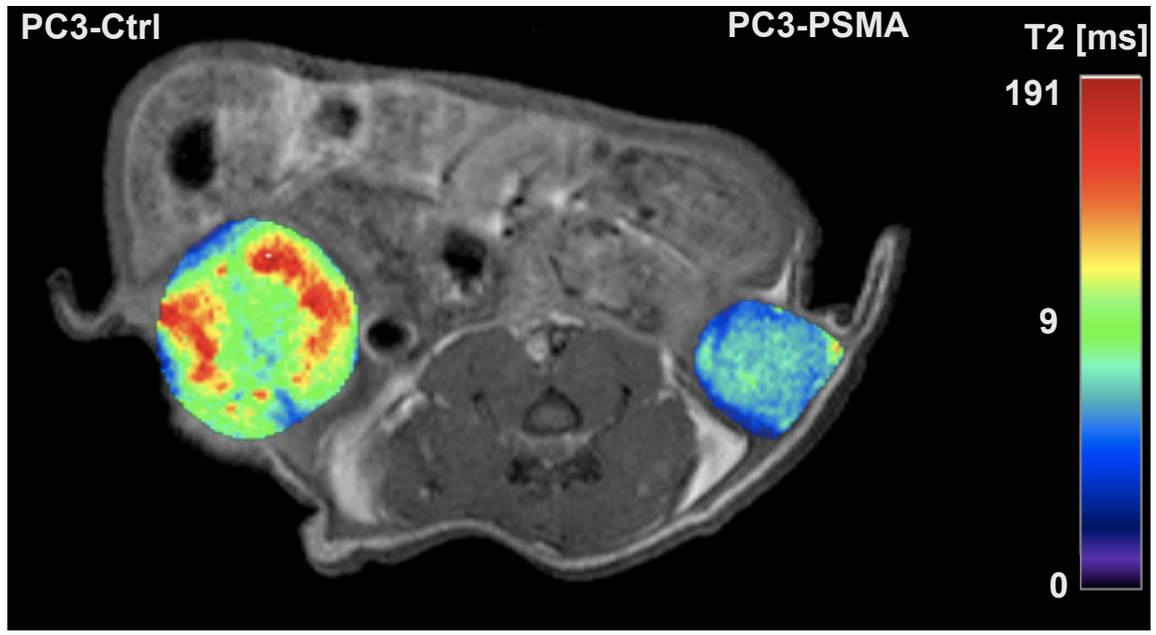
PC3-Ctrl
PC3-PSMA
T2 [ms]
191
9
0

E)

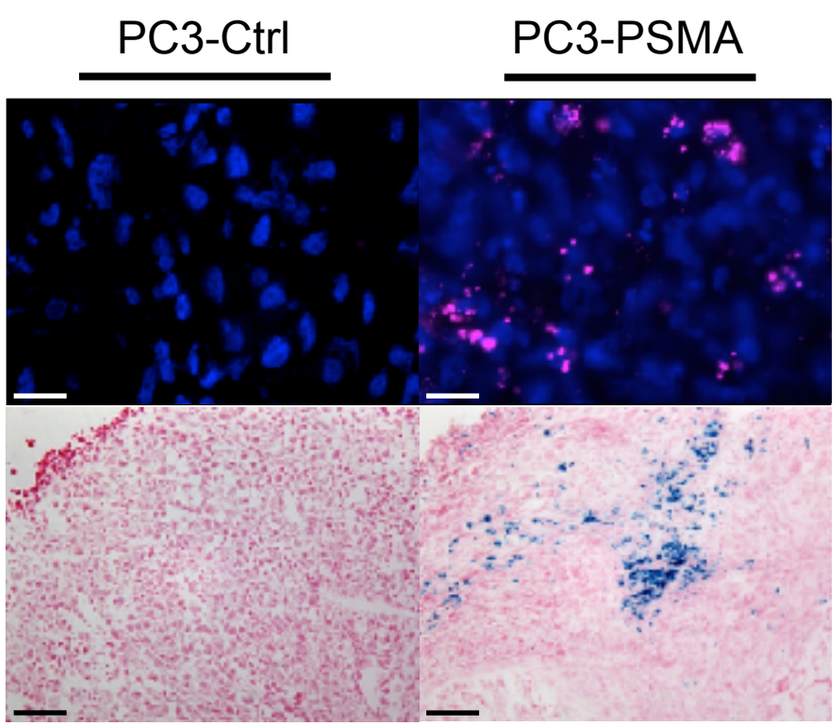
PC3-Ctrl
PC3-PSMA
Fluorescence
H&E/
Prussian Blue

D)

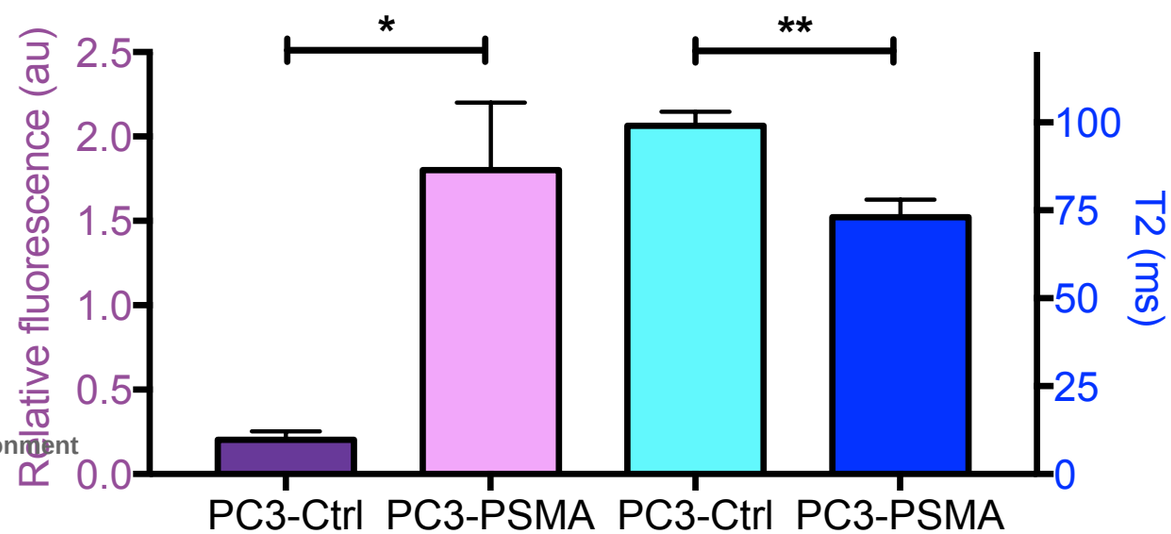
*
**
2.5
2.0
1.5
1.0
0.5
0.0
Relative fluorescence (au)
100
75
50
25
0
T2 (ms)
PC3-Ctrl
PC3-PSMA
PC3-Ctrl
PC3-PSMA

A)

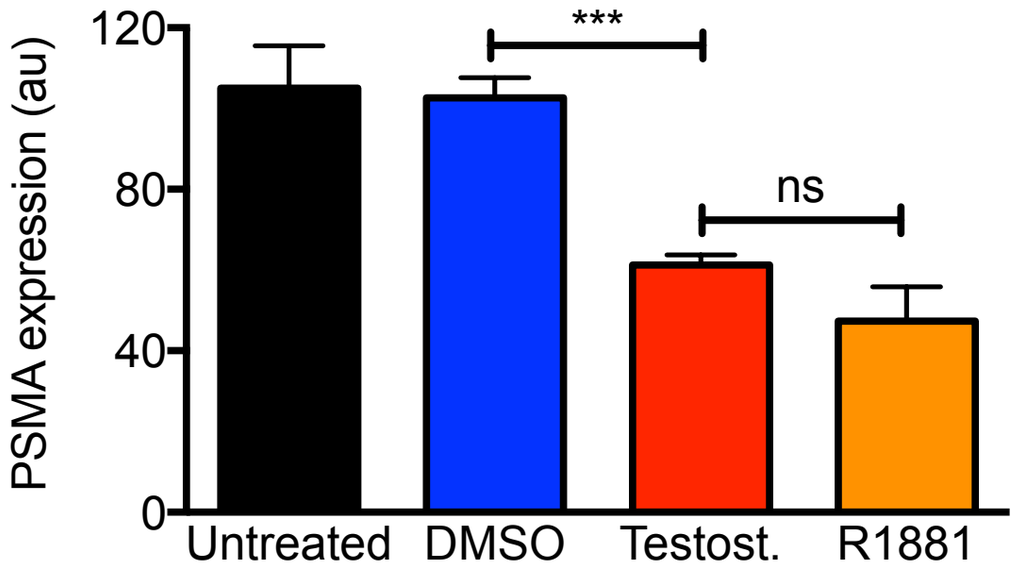
PSMA expression (au)
120
80
40
0
***
ns
Untreated
DMSO
Testost.
R1881

B)

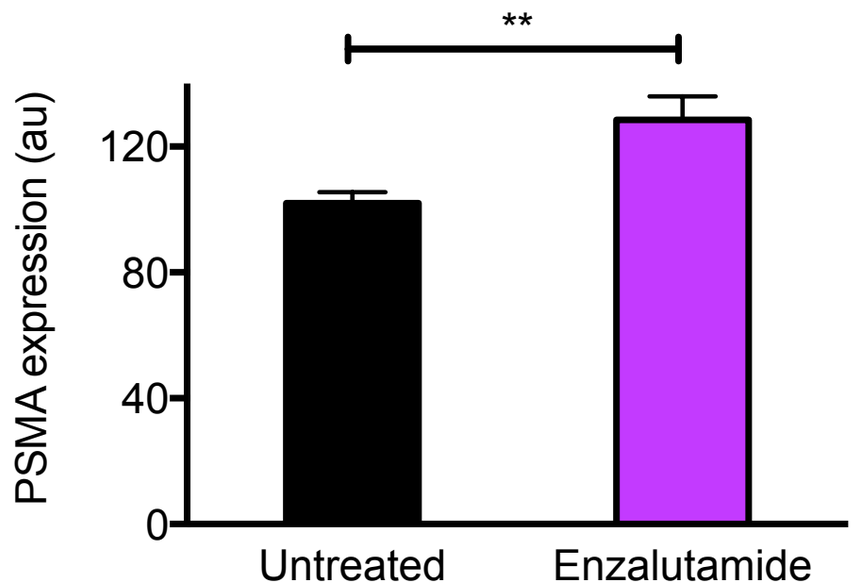
PSMA expression (au)
120
80
40
0
**
Untreated
Enzalutamide

C)

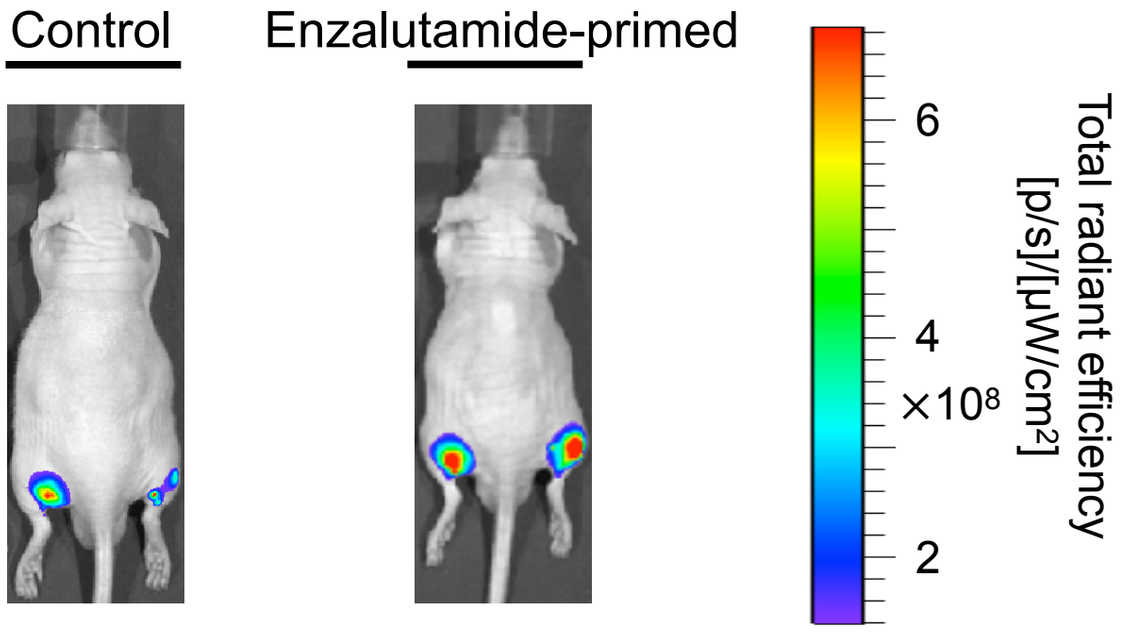
Control
Enzalutamide-primed
6
4
×10⁸
2
Total radiant efficiency
[p/s]/[µW/cm²]

D)

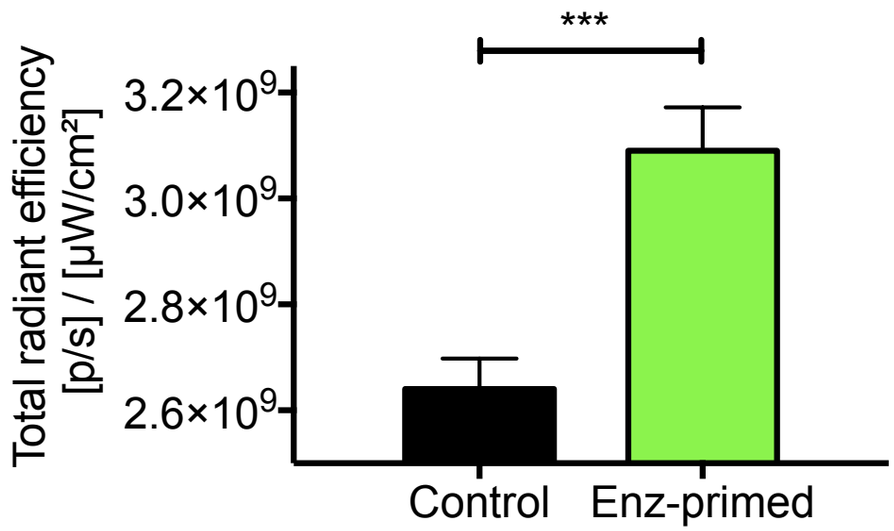
Total radiant efficiency
[p/s] / [µW/cm²]
3.2×10⁹
3.0×10⁹
2.8×10⁹
2.6×10⁹
***
Control
Enz-primed

A)

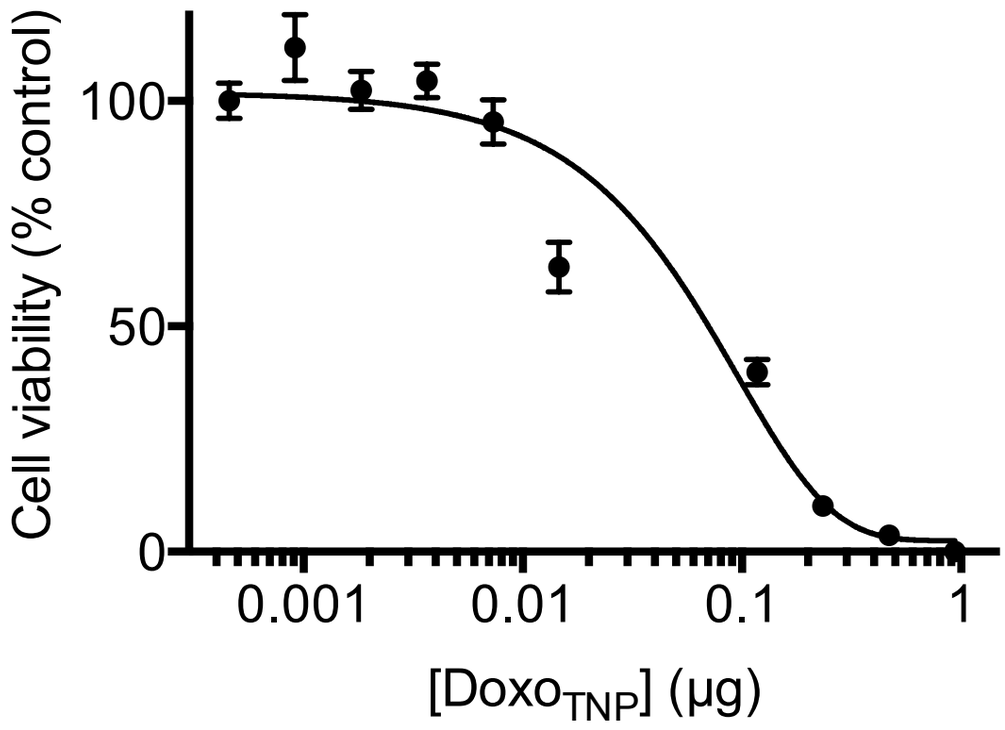
Cell viability (% control)
100
50
0
0.001
0.01
0.1
1
[Doxo$_{TNP}$] (µg)

B)

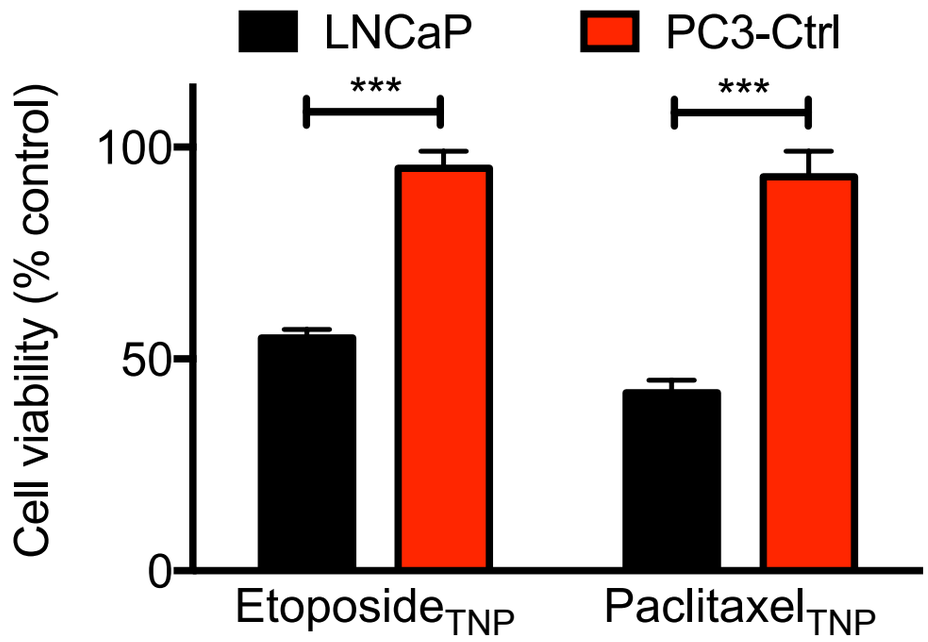
LNCaP
PC3-Ctrl
***
***
Cell viability (% control)
100
50
0
Etoposide$_{TNP}$
Paclitaxel$_{TNP}$

C)

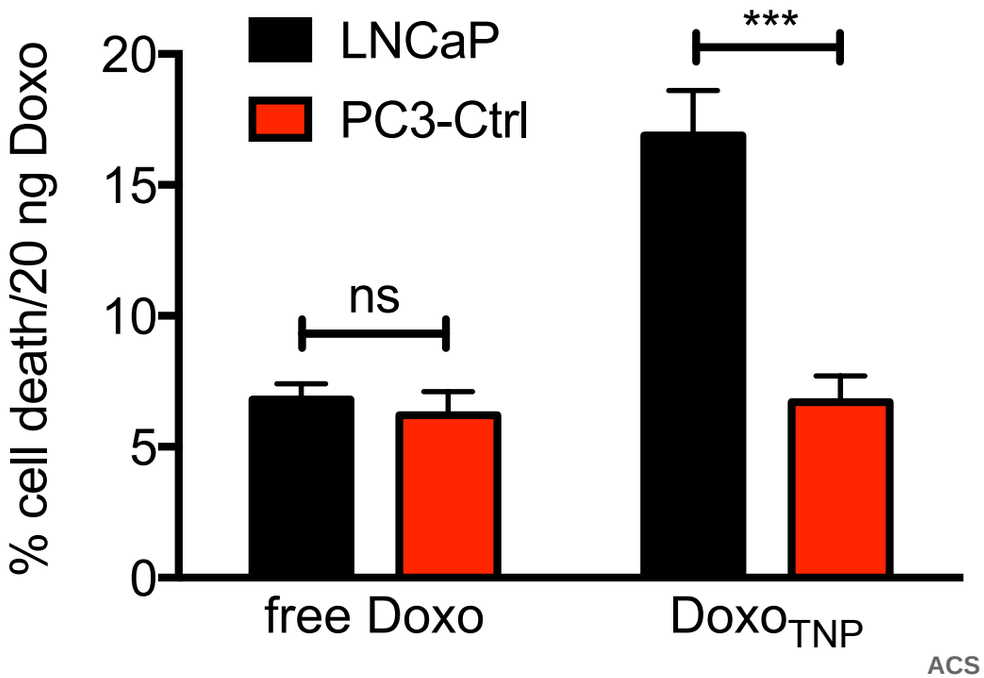
LNCaP
PC3-Ctrl
***
ns
% cell death/20 ng Doxo
20
15
10
5
0
free Doxo
Doxo$_{TNP}$

D)

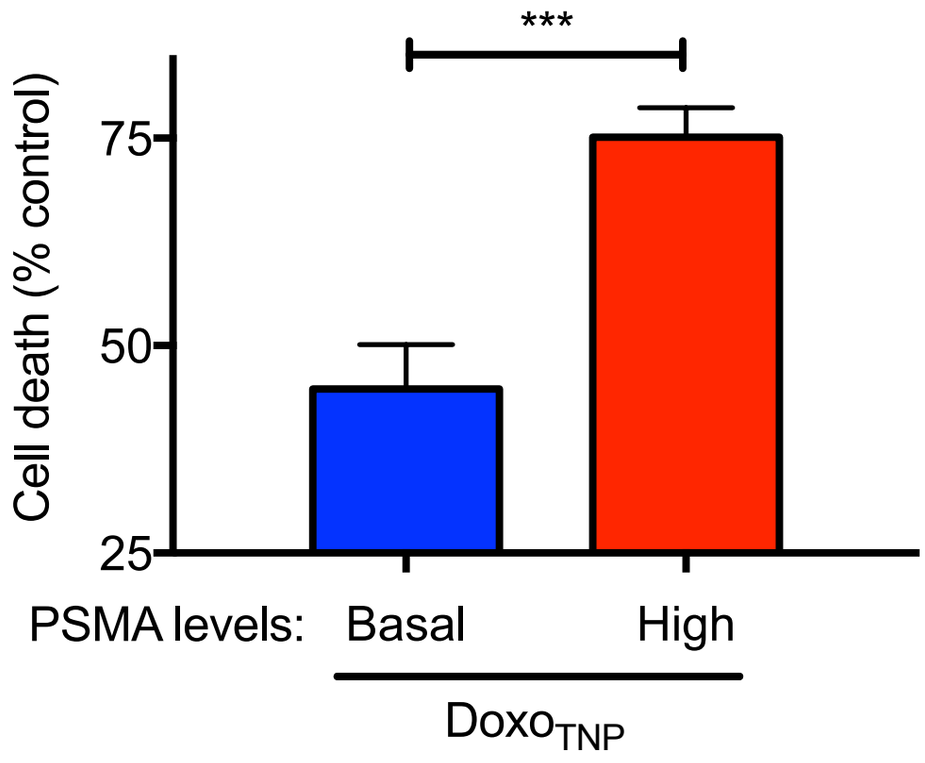
***
Cell death (% control)
75
50
25
PSMA levels:
Basal
High
Doxo$_{TNP}$

A)

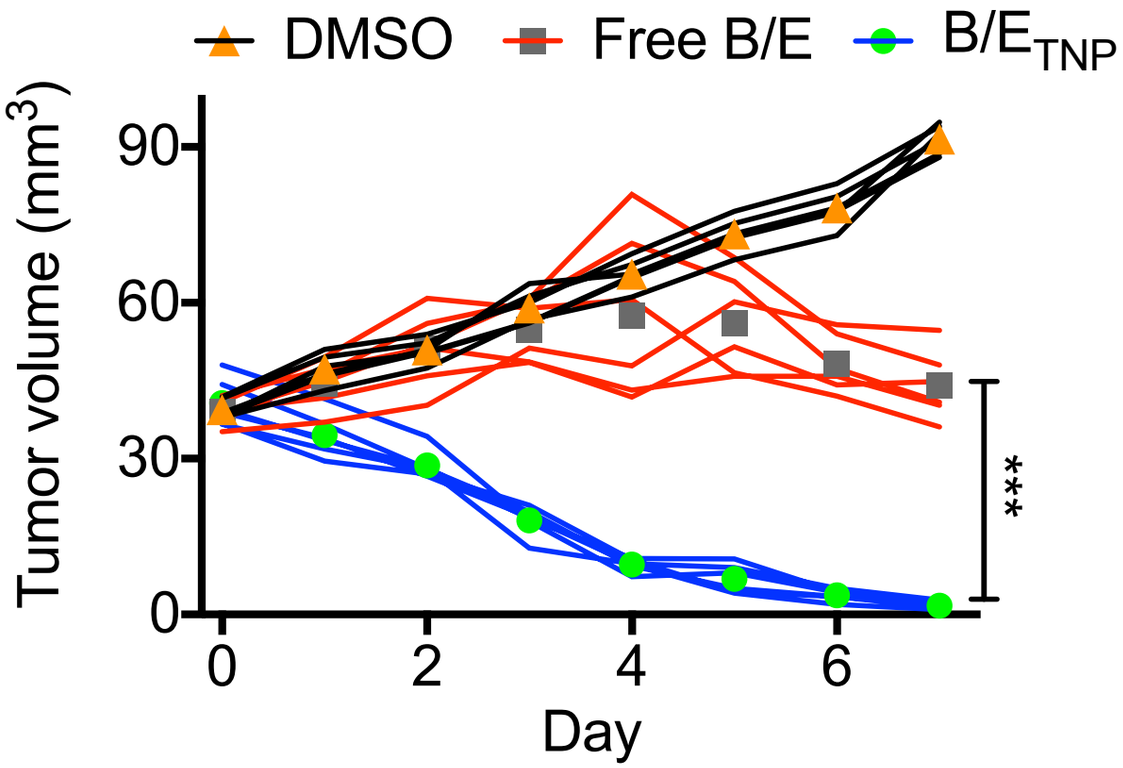
DMSO
Free B/E
B/E$_{TNP}$
Tumor volume (mm^3)
90
60
30
0
0
2
4
6
Day
***

B)

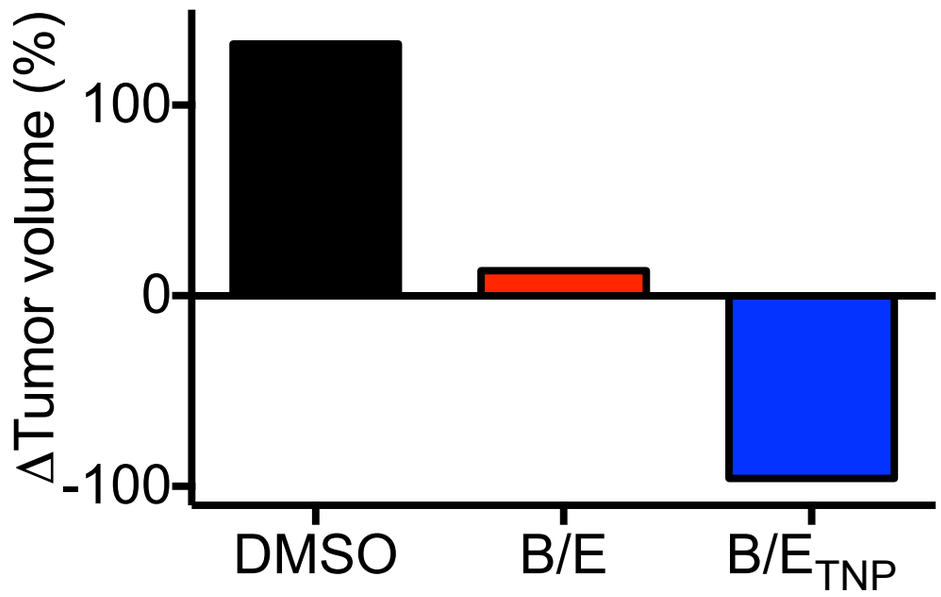
ΔTumor volume (%)
100
0
-100
DMSO
B/E
B/E$_{TNP}$

C)

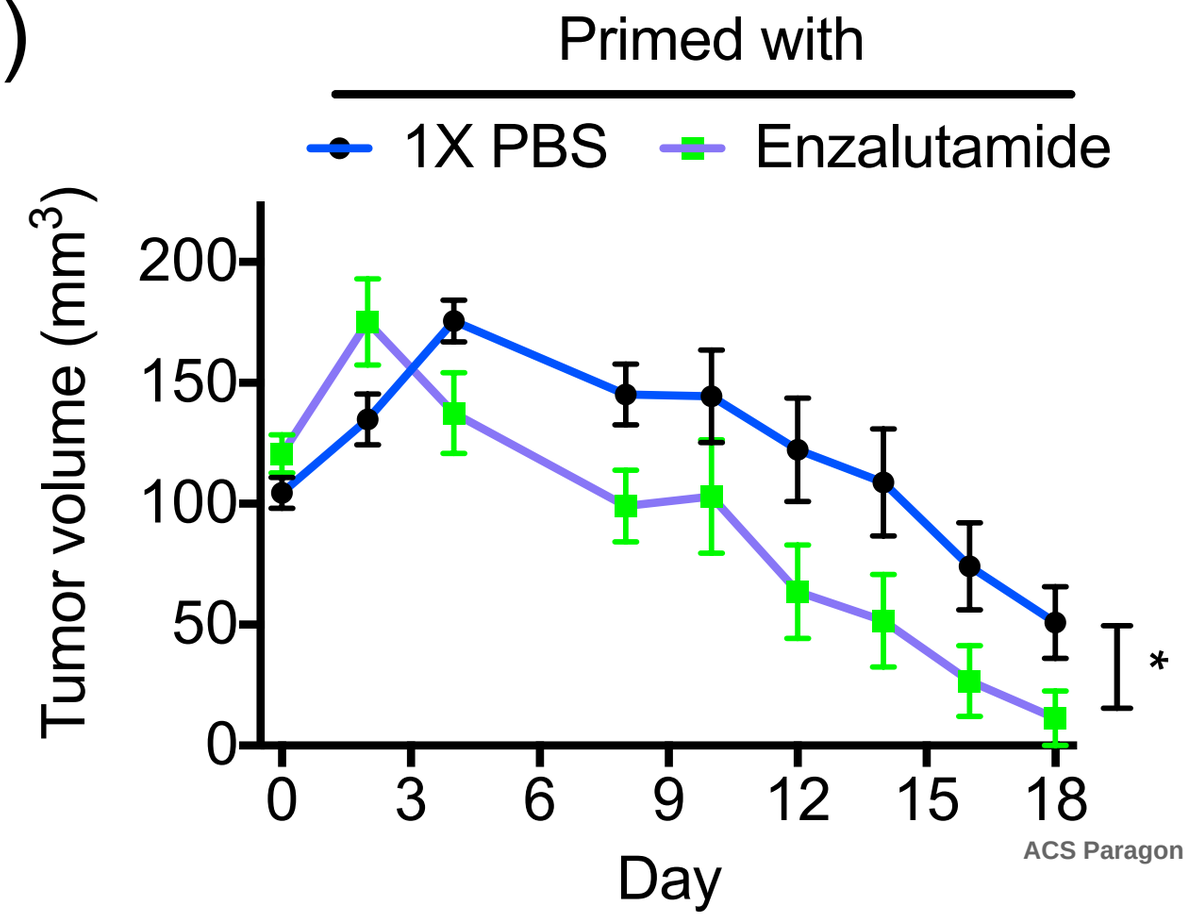
Primed with
1X PBS
Enzalutamide
Tumor volume (mm^3)
200
150
100
50
0
0
3
6
9
12
15
18
Day
*

D)

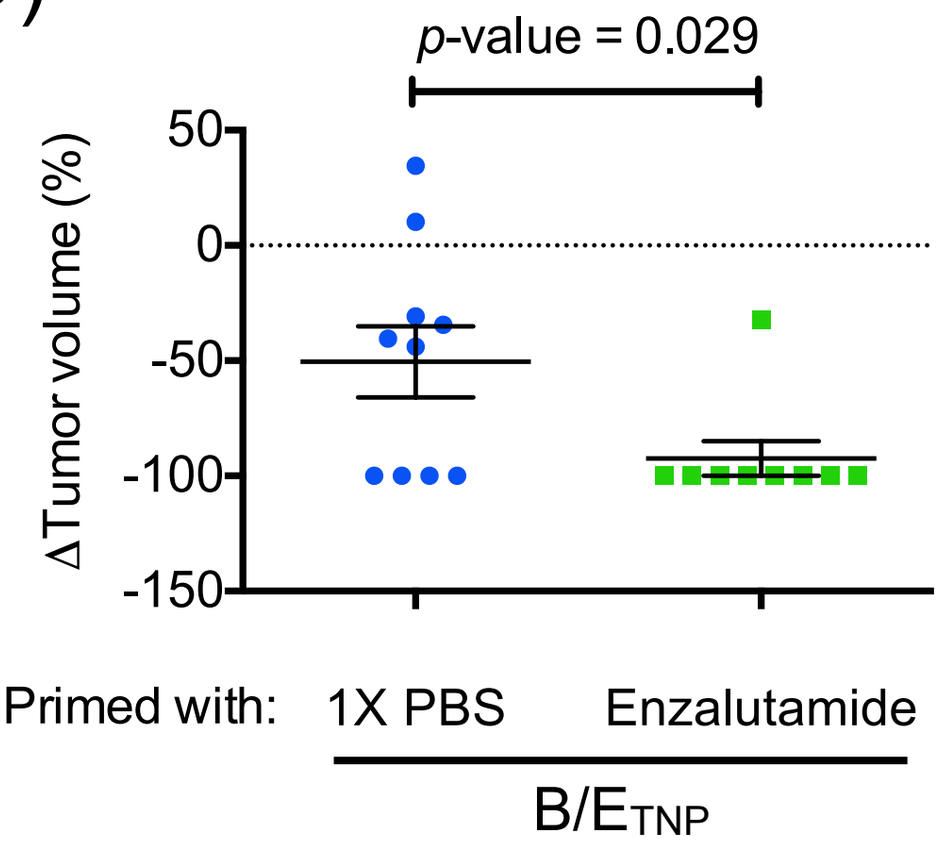
p-value = 0.029
ΔTumor volume (%)
50
0
-50
-100
-150
Primed with:
1X PBS
Enzalutamide
B/E$_{TNP}$

A)

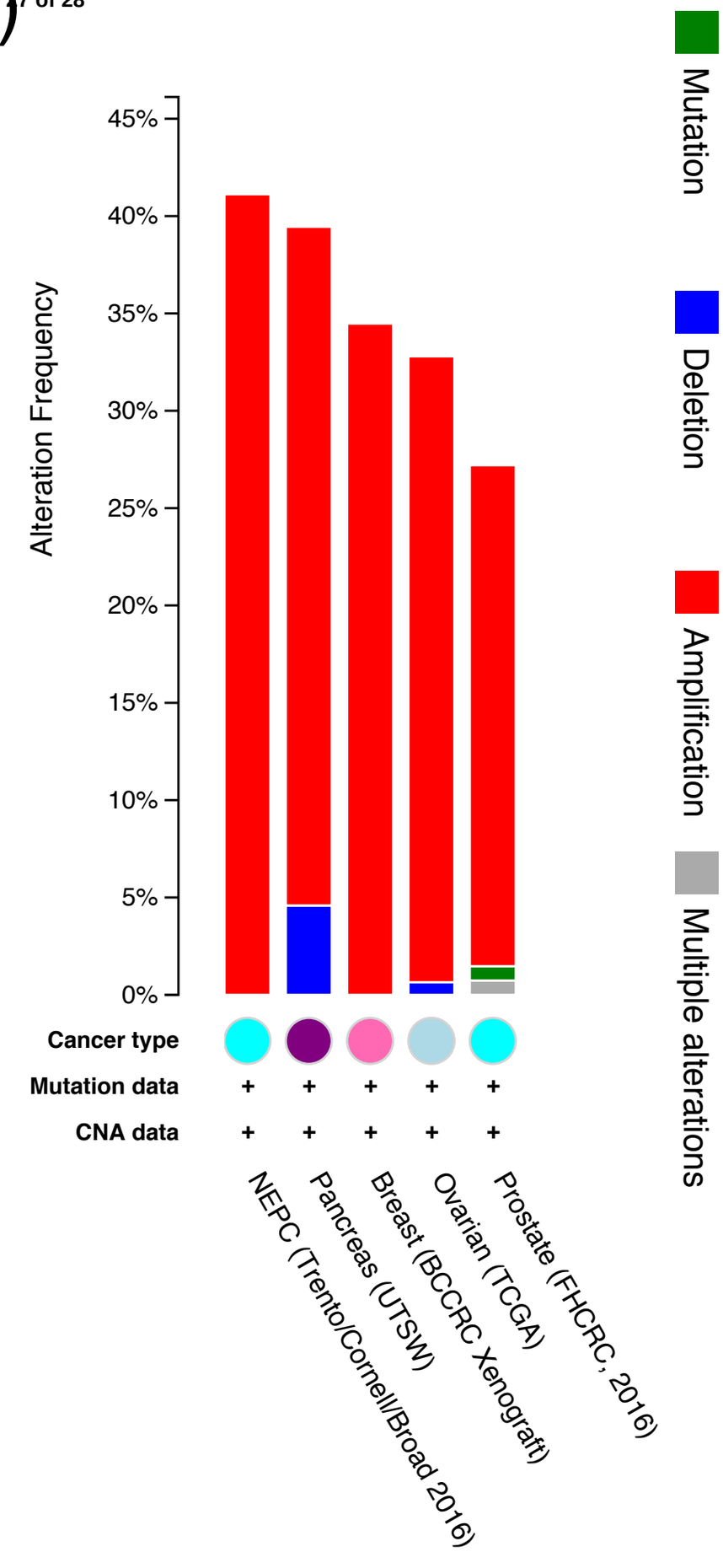
Alteration Frequency
45%
40%
35%
30%
25%
20%
15%
10%
5%
0%
Mutation
Deletion
Amplification
Multiple alterations
Cancer type
Mutation data
CNA data
NEPC (Trento/Cornell/Broad 2016)
Pancreas (UTSW)
Breast (BCCRC Xenograft)
Ovarian (TCGA)
Prostate (FHCRC, 2016)

B)

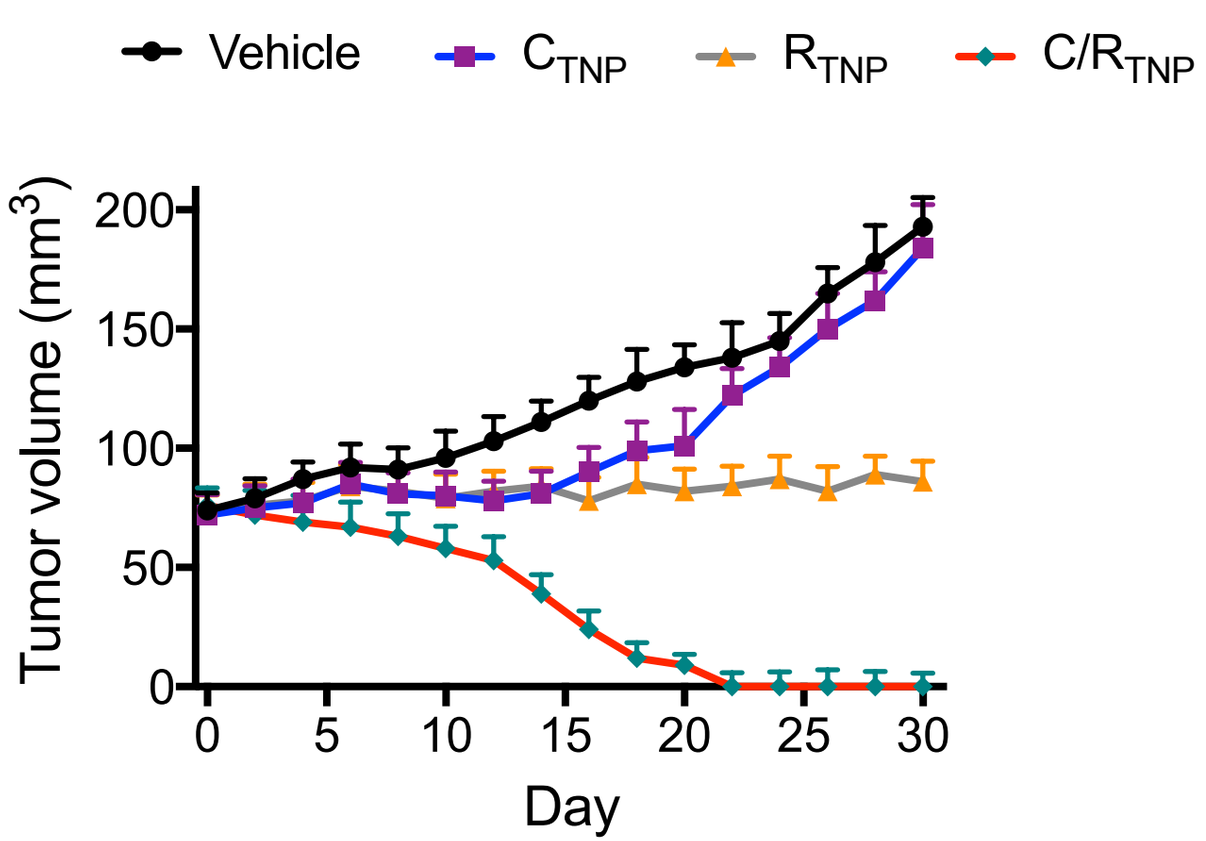
Vehicle
C_TNP
R_TNP
C/R_TNP
Tumor volume (mm3)
200
150
100
50
0
0
5
10
15
20
25
30
Day

C)

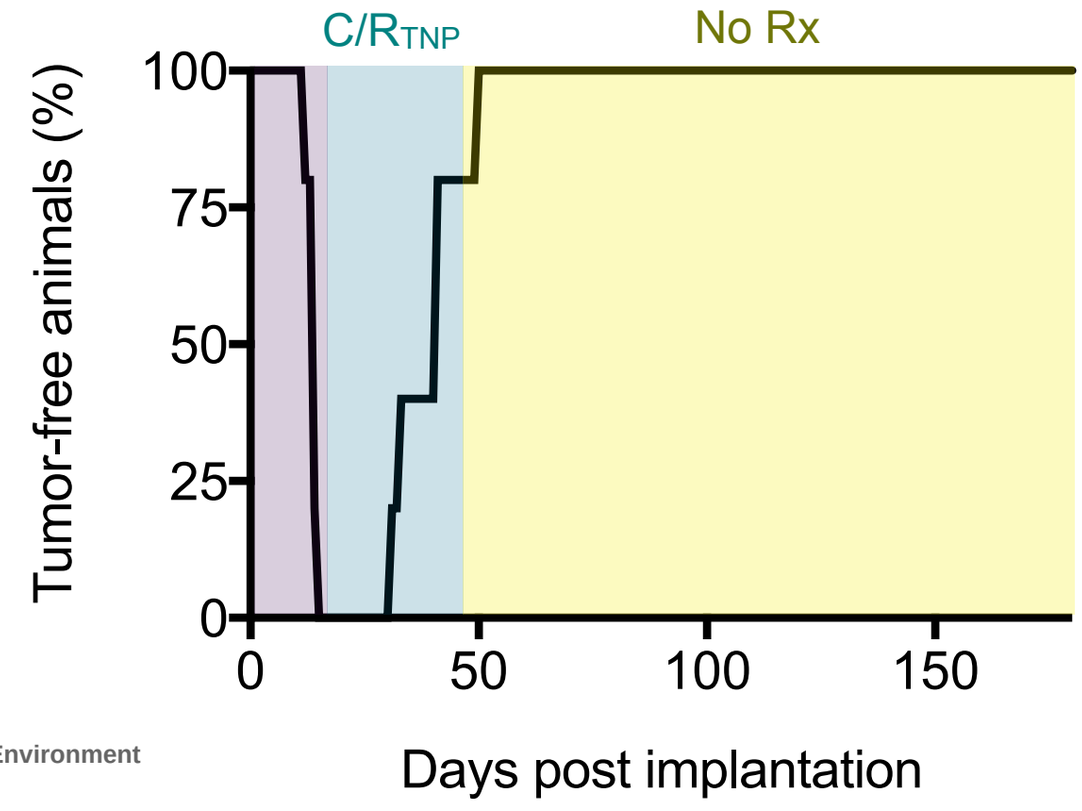
C/R_TNP
No Rx
Tumor-free animals (%)
100
75
50
25
0
0
50
100
150
Days post implantation

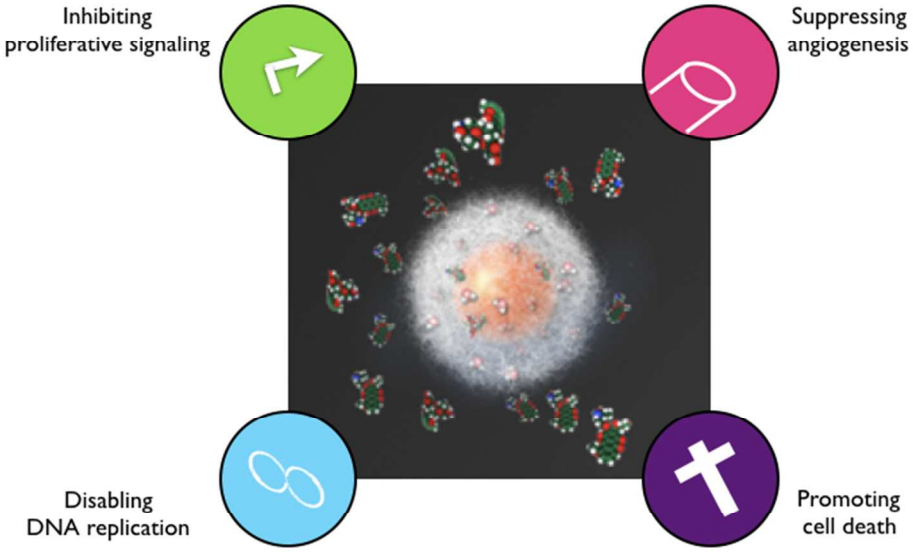

Figure for TOC

261x173mm (72 x 72 DPI)